Catalytic wet torrefaction of biomass waste into bio-ethanol, levulinic acid, and high quality solid fuel

Andrii Kostyniuk [a,*], Blaž Likozar [a,b,c,d]

[a] Department of Catalysis and Chemical Reaction Engineering, National Institute of Chemistry, Hajdrihova 19, Ljubljana 1001, Slovenia
[b] Faculty of Polymer Technology, Slovenj Gradec 2380, Slovenia
[c] Pulp and Paper Institute, Bogišićeva 8, Ljubljana 1000, Slovenia
[d] Faculty of Chemistry and Chemical Technology, University of Ljubljana, Večna pot 113, Ljubljana 1000, Slovenia

ABSTRACT

Creating a sustainable society hinges on efficient chemical and fuel production from renewable cellulosic biomass, necessitating the development of innovative transformation routes from cellulose. In this investigation, we unveil a pioneering chemocatalytic method, utilizing an H-ZSM-5 catalyst within a batch reactor under a nitrogen atmosphere, for the simultaneous one-pot generation of levulinic acid (LA) and/or ethanol during wet torrefaction (WT) of wood cellulose pulp residue (WCPR), yielding high-quality solid fuel. WT parameters include a temperature range of 180 to 260 °C, H_2O/WCPR = 10, and reaction durations of 15 to 60 min. Optimal conditions for bio-ethanol production are identified at 180 °C and 15 min, achieving an outstanding 89.8 % selectivity with H-ZSM-5 catalyst. Notably, 69.5 % LA formation occurs at 240 °C after 60 min. Hydrochar assessments include higher heating values (HHVs), decarbonization (DC), dehydrogenation (DH), deoxygenation (DO), enhancement factor, carbon enrichment, surface area, pore diameter, weight loss, and yields of solid, carbon, hydrogen, and energy. The highest carbon content of 76.7 % is attained at 260 °C for 60 min, resulting in an HHV of 29.0 MJ/kg, an enhancement factor of 1.44, and carbon enrichment of 1.59, with a sequence of element removal as DO > DH > DC. A proposed reaction pathway elucidates WT of WCPR with the H-ZSM-5 catalyst, emphasizing the direct cellulose conversion into hydroxyacetone and subsequent ethanol generation through C–C cleavage of hydroxyacetone. Through this research approach, both ethanol and LA can be produced efficiently from renewable cellulosic biomass, offering a novel pathway to reduce dependence on fossil resources.

1. Introduction

The depletion of non-renewable fossil resources has led to global issues such as energy shortages and environmental degradation, such as air pollution and global warming [1]. Fortunately, biomass, the sole source of renewable carbon, shows significant promise for conversion into valuable biochemicals and biofuels, offering a path to tackle both energy and environmental challenges [2]. Biomass possesses the capability to undergo various thermochemical conversion technologies, resulting in solid, liquid, and gaseous biofuels [3]. These biofuels offer a sustainable and environmentally friendly energy source. With its nearly carbon–neutral properties and widespread natural availability, biomass has the potential to significantly reduce fossil fuel consumption and environmental pollution, especially in terms of mitigating greenhouse gas emissions [4].

Biomass, comprising approximately 40 to 60 % cellulose, 15 to 30 % hemicellulose, and 10 to 25 % lignin, alongside inorganic minerals and organic extractives (ash), faces inherent limitations when compared to coal [5]. These challenges encompass its heterogeneous nature, lower calorific value, higher moisture content, hydrophilic properties, poor grindability, handling and storage difficulties, and lower energy density relative to fossil fuels, collectively impacting its viability as an alternative energy source [6]. Moreover, biomass combustion tends to be inefficient and costly, prompting the necessity for thermal conversion processes to overcome these limitations and produce high-density biofuels. Various thermal conversion processes, including torrefaction, pyrolysis, hydrothermal liquefaction, gasification, and combustion, are employed to transform biomass into valuable energy resources [3]. Notably, torrefaction stands out as a significant green thermochemical process for producing solid biofuel, known as biochar or hydrochar,

from diverse biomass resources like woody and non-woody residue, agricultural waste, agro-industrial waste, and municipal solid waste [7]. Hydrochar, recognized for its versatility, finds applications in greenhouse gas sequestration, cost-effective adsorbents, soil enhancement, catalyst support, and more [8]. Torrefied biomass, sharing properties similar to coal, emerges as a potential partial substitute. Posttorrefaction, biomass can be densified through briquetting or pelletizing using standard equipment, effectively increasing material density and enhancing hydrophobic characteristics [9]. Torrefaction, a mild pyrolysis process for thermal pretreatment, aims to improve higher heating values and energy densities, reduce atomic O/C and H/C ratios, lower moisture content, enhance water resistance, increase grindability and reactivity, and achieve uniform properties [10]. Dry torrefaction (DT), conducted in an oxygen-free environment with low heating rates (generally below 50 °C/min), occurs within a temperature range of 200–300 °C [11].

Wet torrefaction (WT), commonly known as hydrothermal torrefaction, is a high-pressure (up to 4.6 MPa) thermal pretreatment process carried out in hot compressed water under inert conditions, typically at temperatures ranging from 180 to 260 °C [12,13]. WT offers several advantages over DT. WT requires notably lower temperatures and shorter holding times than DT to achieve equivalent solid yields, resulting in higher energy yields, greater higher heating value (HHV), and improved hydrophobicity. As a result, WT proves to be a more effective method for biomass energy densification and conservation compared to DT. Moreover, WT holds significant potential as a cost-efficient approach for producing cleaner biomass fuels from inexpensive, lower-quality biomass resources. WT can efficiently handle wet, and even extremely wet, biomass materials, which pose challenges for DT [14].

Cellulose, the main component of lignocellulose, composed of C6 sugars, is an ideal raw material for ethanol production; nevertheless, the direct conversion of abundant non-edible cellulose into ethanol *via* chemical catalysis remains a substantial challenge [15]. Bio-ethanol is a key renewable low-carbon fuel that plays a pivotal role in meeting energy demands, reducing greenhouse gas emissions, and serving as a valuable partial substitute for gasoline in various sectors, including chemical industries, medicine, healthcare, and agriculture production. Commercial ethanol is commonly produced through either classical fermentation (a biological method) or gasification followed by syngas conversion (a thermochemical method), but both methods face technical challenges and complex processes, resulting in higher production costs [16]. On the other hand, a chemocatalytic approach using a solid acid catalyst presents an alternative avenue for ethanol production from cellulose, with a particular preference for converting cellulose and its derivatives into ethanol. Solid catalysts offer economic and environmental advantages. They are favored in industrial applications for their straightforward recovery and recyclability, making them a preferred choice [17].

Only a few catalysts have been used in the production of ethanol through catalytic biomass/cellulose conversion [15,18–20]. Liu et al. [18] successfully synthesized ethanol through a one-pot cellulose hydrogenolysis process, utilizing graphene-layer-encapsulated nickel (Ni@C) catalysts with the assistance of H_3PO_4 in water. This reaction took place at 200 °C for 3 h in a 100 mL autoclave with stirring, resulting in an impressive 69.1 % ethanol yield under a 5.5 MPa H_2 atmosphere. In a similar vein, Yang and his co-authors [19] also generated ethanol with a yield as high as 43.2 % using a one-pot cellulose conversion method, employing the Mo/Pt/WO$_x$ catalyst in a 50 mL autoclave at 245 °C for 2 h with a purged 6 MPa H_2 atmosphere. Wu and his colleagues [15] performed a one-step conversion of cellulose into ethanol, employing the Pt/WO$_x$ and hollow Pt@HZSM-5 catalysts, yielding 54.4 % ethanol in a 100 mL autoclave at 245 °C while stirring for 4 h with 4 MPa H_2. Furthermore, Li et al. [20] achieved an outstanding 87.5 % ethanol yield from 1 wt% cellulose through a one-pot process using the Ru-WO$_x$/HZSM-5 catalyst at 235 °C, stirring for 20 h in water under a 3 MPa H_2 atmosphere.

Levulinic acid (LA) or also known as 4-oxopentanoic acid or gamma ketovaleric acid, a versatile renewable C5 platform molecule with various potential industrial applications, serves as the foundation for the production of a wide range of high-volume chemicals and fuels [21]. However, its commercial production currently relies on homogeneous acid catalysts like sulfuric acid, which contributes to increased production costs due to its expense, the need for neutralization, and the challenges associated with separating it from levulinic acid [17].

Regarding the formation of LA from cellulose over solid acid catalysts, there have been several studies [17,22–25]. Weingarten and colleagues [17] achieved a successful conversion of cellulose into LA, utilizing Amberlyst 70 as a catalyst at a temperature of 220 °C for 30 min. This resulted in a maximum yield of LA, reaching 28 % of the theoretical yield in reactor vessels with capacities of both 100 and 160 mL, operating under a helium atmosphere at a pressure of 4–5 MPa. In a subsequent study, Chen et al. [23] employed Amberlyst 36 as the catalyst within a temperature range of 120–150 °C and accelerated the production of LA, achieving yields between 13 % and 17 % in just 5 min, utilizing microwave heating. Meanwhile, Xu et al. [22] obtained LA using a carbon foam-supported heteropolyacid catalyst. They achieved a cellulose conversion rate of 89.4 % and a LA yield of 60.9 % at a reaction temperature of 180 °C for a duration of 4 h, employing a stainless steel reactor. In another approach, Xiang and colleagues [24] harnessed ETS-10 zeolite and accomplished a high LA yield of 91.0 % while conducting the reaction in an H_2 atmosphere.

In this investigation, we present an innovative chemocatalytic method for the simultaneous one-pot generation of LA and/or ethanol during WT of wood cellulose pulp residue (WCPR), utilizing a H-ZSM-5 zeolite catalyst and yielding high-quality solid fuel within a batch reactor under a nitrogen atmosphere. This process was carried out under varying conditions of reaction time and temperature, with water serving as the reaction medium. In this investigation, our main goal was to optimize the production of hydrochar, aiming for an increase in both higher heating value and carbon content. Concurrently, we set out to obtain valuable liquid by-products, such as ethanol and LA, and delve into the intricate mechanisms underlying these transformations. In addition to these objectives, we conducted an extensive analysis of both WCPR and the resulting hydrochar generated during the WT process. To achieve this, we employed a range of characterization techniques, including X-ray diffraction (XRD), scanning electron microscopy (SEM), Brunauer-Emmett-Teller analysis (BET), elemental analysis encompassing carbon, hydrogen, nitrogen, oxygen, and sulfur (CHN(O)S), as well as thermogravimetric analysis (TGA).

2. Experimental section

2.1. Materials

The H-ZSM-5 zeolite catalyst with a SiO_2/Al_2O_3 ratio of 30 was acquired from the commercial supplier Zeolyst International (Conshohocken, PA, USA). Prior to use, the zeolite underwent a calcination process at 550 °C (10 °C/min) in the air for 6 h to eliminate impurities. Others chemical reagents, calibration standards, and gases used in this study were sourced commercially and did not require additional purification. The specific chemicals and their respective suppliers are as follows: ethanol (>99.8 %, Merck, Germany), levulinic acid (99.5 %, Merck, Germany), hydroxyacetone (99.5 %, Merck, Germany), 5-hydroxymethylfurfural (>97 wt%, Carbosynth, UK), 5-methylfurfural (99 wt%, Merck, Germany), furfural (>99 wt%, Merck, Germany), methanol (>99.9 %, Merck, Germany), guaiacol (99.5 %, Merck, Germany), 2,3-butanedione (99 %, Merck, Germany), phenol (≥98.5 %, Merck, Germany), 2-butanone (99.5 %, Merck, Germany), acetone (>99.5 %, Merck, Germany), acetoin (>99.5 %, Merck, Germany), acetic acid (>99.7 %, Merck, Germany), cyclopentenone (>99 %, Merck, Germany), acetylacetone (>99 %, Merck, Germany), 2,5-

hexanedione (>99.5 %, Merck, Germany), hydrogen (5.0, Messer, Germany), nitrogen (5.0, Messer, Germany), helium (5.0, Messer, Germany). The feedstock, referred to as WCPR (wood cellulose pulp residue), was provided by the biotechnology company Vertoro (Geleen, Netherlands). A detailed composition of WCPR can be found in Table S1.

2.2. Analysis

The vario EL cube elemental analyzer from Elementar in Hanau, Germany, was used in CHNS mode to determine the levels of carbon, hydrogen, nitrogen, and sulfur. Carbon, hydrogen, and nitrogen were detected using a thermal conductivity detector, while sulfur was measured with an infrared detector. To set up the instrument, a low-level standard provided by Elementar, containing 67.65 % carbon, 4.95 % hydrogen, 0.72 % nitrogen, and 0.84 % sulfur, was employed for calibration. The combustion tube was heated to 1150 °C, and the reduction tube to 850 °C. The CHNOS content was ultimately assessed on a dry basis after subtracting the water content.

$$O = 100\% - C\% - H\% - N\% - S\% - moisture\% - ash\% - Si\% - Al\% \quad (1)$$

To study the pyrolysis of dehydrated and torrefied cellulose, a TGA-IR (Thermogravimetric Analysis-Infrared Spectrometry) system known as Spectrum 3 with EGA 4000, manufactured by PerkinElmer, was utilized. Each analysis involved employing approximately 10 mg of the sample, which underwent heating from 40 to 750 °C at a rate of 10 °C/min. Nitrogen gas with a purity exceeding 99.999 %, flowing at a rate of 20 mL/min, was employed as the carrier gas. The experimental outcomes from the TGA were automatically recorded using a computer.

The determination of moisture, volatile matter, fixed carbon, and ash content in both untreated and wet torrefied WCPR was carried out using proximate analysis, employing a thermal gravimetric analyzer, specifically the Spectrum 3 with EGA 4000 by PerkinElmer. The American Society for Testing and Materials (ASTM) standards E-871, E-1755, and E-872 were employed for assessing moisture, ash, and volatile matter, respectively [26,27]. In this analytical process, approximately 10 mg of the sample underwent controlled heating within a nitrogen atmosphere. The process commenced at 40 °C and progressed to 120 °C, with a 10 min pause to measure the moisture content (MC, wt%). Subsequently, a heating rate of 50 °C/min was applied until reaching 800 °C, with a 20 min hold to determine the volatile matter (VM, wt%). To determine the ash content (Ash, wt%), the cooling phase was initiated with a cooling rate of –50°/min until it reached 450 °C, at which point the nitrogen atmosphere was replaced with air. Following this, a new heating ramp of 25 °C/min was initiated, continuing until 800 °C, and then maintained isothermally for 3 min. The fixed carbon content (FC, wt%) was calculated using Eq. (2) as follows:

$$FC = 100 - (MC + Ash + VM) \quad (2)$$

Eq. (3) was used to calculate the higher heating value (HHV) for both the WCPR and WT + ZSM-5 samples [28].

$$HHV\ (MJ/kg) = 0.3491 \times C + 1.1783 \times H - 0.1034 \times O + 0.1005 \times S - 0.0151 \times N - 0.0211 \times A \quad (3)$$

In Eq. (3), C, H, O, S, N and A represent the carbon, hydrogen, oxygen, sulfur, nitrogen, and ash contents, respectively, obtained from the elemental analysis and expressed as weight percentages on a dry basis. The use of these equations enables the calculation of both the higher and lower heating values of the biomass. This, in turn, offers a comprehensive understanding of the energy properties of the biomass during torrefaction conditions. The formulas used to determine the solid yield and energy yield of the torrefied samples were as follows:

$$Y_{solid} = (m_{poduct}/m_{feedstock}) \times 100\% \quad (4)$$

$$Y_{energy} = ((Y_{solid} \times HHV_{product})/HHV_{feedstock}) \times 100\% \quad (5)$$

within these equations, Y_{solid} represents the solid yield, and Y_{energy} corresponds to the energy yield. The variables $m_{feedstock}$ and $m_{product}$ signify the mass of the initial samples and the solid product following torrefaction, respectively. $HHV_{feedstock}$ and $HHV_{product}$ denote the higher heating value (in MJ/kg) of the initial samples and the solid product after torrefaction, respectively [29]. The enhancement factor was defined as follows [30]:

$$Enhancement\ factor = HHV_{product}/HHV_{feedstock} \quad (6)$$

Carbon yield (Y_C) and hydrogen yield (Y_H) were calculated as follow:

$$Y_C\ (wt\%) = Y_{solid}\ (wt\%) \times (C_{product}/C_{feedstock}) \quad (7)$$

$$Y_H\ (wt\%) = Y_{solid}\ (wt\%) \times (H_{product}/H_{feedstock}) \quad (8)$$

where $C_{product}$, $H_{product}$ and $C_{feedstock}$, $H_{feedstock}$ are the dry ash free carbon and hydrogen content of the WT + ZSM-5 and WCPR samples, respectively.

Decarbonization (DC), dehydrogenation (DH), and deoxygenation (DO) are three metrics used to measure the reduction in the mass of carbon, hydrogen, and oxygen during biomass torrefaction [30]. DC quantifies the percentage of carbon loss in the biomass due to WT and can be determined using the following formula:

$$DC\ (wt\%) = 100 - Y_{solid}\ (wt\%) \times (C_{product}/C_{feedstock}) \quad (9)$$

DH and DO can be similarly calculated using the same procedure as DC.

$$DH\ (wt\%) = 100 - Y_{solid}\ (wt\%) \times (H_{product}/H_{feedstock}) \quad (10)$$

$$DO\ (wt\%) = 100 - Y_{solid}\ (wt\%) \times (O_{product}/O_{feedstock}) \quad (11)$$

where $O_{product}$ and $O_{feedstock}$ are the dry ash free oxygen content of the WT + ZSM-5 and WCPR samples, respectively.

A metric known as carbon enrichment (CE), employed to evaluate the extent of carbonization in WT + ZSM-5, is defined as follows:

$$CE = C_{product}/C_{feedstock} \quad (12)$$

Lastly, the weight loss (WL) or conversion of WT + ZSM-5 is expressed as follows:

$$WL\ (wt\%) = 100 - Y_{solid} \quad (13)$$

N_2 adsorption–desorption at the temperature of liquid nitrogen (77 K) was performed using a Micromeritics micropore analyzer, specifically the Micromeritics ASAP 2020 instrument. This analysis was conducted to determine the BET surface area for both the untreated and moistened torrefied samples. Furthermore, a high-resolution scanning electron microscopy (HR-SEM) inspection was carried out on WCPR and wet torrefied WCPR samples, using the FE-SEM SUPRA 35-VP instrument manufactured by Carl Zeiss.

X-ray diffraction (XRD) analysis was carried out using the PANalytical XpertPro powder X-ray diffraction instrument. CuKα1 radiation with a wavelength of 1.54056 Å was employed at 45 kV and 40 mA, covering a scanning range from 5 to 50° with increments of 0.033°. To assess the impact of WT on the overall crystalline structure of the feedstock, the crystallinity index (CI) was determined using the Segal method [31]. This method involved evaluating the intensities of the (2 0 0) plane (I_{200}) at $2\theta = 22.4°$ and the amorphous regions (I_{am}) at $2\theta = 18.0°$, which corresponds to the minimum point between the 200 and 110 peaks [32,33].

$$CI = ((I_{200} - I_{am})/I_{200}) \times 100\% \quad (14)$$

The crystallite size (CS) was determined using the Scherrer equation [34].

$$CS = (\kappa \times \lambda)/(\beta \times \cos\theta) \quad (15)$$

within the Scherrer equation, the variable κ signifies the Scherrer constant (with a value of 0.90), λ represents the X-ray wavelength (0.15406 nm), β denotes the full width at half maximum (FWHM) of the (200) peak, and θ specifies the diffraction angle for the (200) plane [35].

The structural characteristics of H-ZSM-5 zeolite catalyst were determined by various methods and are listed in Table S2. Table S3 displays the acid properties of the H-ZSM-5 zeolite catalyst, which were assessed through the analysis of temperature-programmed desorption of ammonia (NH$_3$–TPD). This investigation utilized a Micromeritics Autochem 2920 II apparatus equipped with a Pfeiffer Vacuum Thermostar quadrupole mass spectrometer. Additionally, pyridine adsorption diffuse-reflection infrared spectroscopy (Pyridine–DRIFTS) was performed using a Frontier IR spectrometer (Perkin Elmer) equipped with an MCT detector and the DiffusIR® accessory from Pike Scientific [36].

2.3. Experimental apparatus and procedure

The WT process for WCPR reactions was carried out using a stainless steel autoclave consisting of six Parr 5000 Multiple Reactor System vessels, each with a capacity of 75 mL. These vessels were equipped with real-time pressure and temperature control regulators, as illustrated in Fig. S1. Each vessel has an inside diameter of 1.50 in., inside depths of 2.69 in. (with a flat gasket) and 2.50 in. (with an O-ring), a weight of 6 lb (including head-mounted valves), and a maximum temperature and pressure rating of 300 °C and 200 bar, respectively. A magnetic stirring bar rotating at 800 rpm was employed to ensure thorough mixing of the reaction mixture. Each reactor was loaded with precisely 3.0 g of WCPR. In the case of the heterogeneously catalyzed reaction, 1.0 g of H-ZSM-5 zeolite with a SiO$_2$/Al$_2$O$_3$ ratio of 30 was introduced into the reactor vessel. The electric heating temperature was meticulously regulated by the temperature control system, and the temperature within the reactor was continuously monitored using an inline thermocouple. The official start of the reaction occurred when the target reaction temperature was achieved. After the reaction, the autoclave was promptly cooled in an ice bath. The separation of solid catalyst and product solutions was accomplished through filtration, and the product solutions were collected using a 0.22 μm membrane HPLC filter. After the separation procedure, the hydrochars were dried overnight at 105 °C. The collected liquid products underwent offline analysis using a gas chromatography-mass spectrometry system, specifically, an Agilent GC-7890A coupled with an Agilent 5977B GC/MSD. This system featured a DB–WAX Ultra Inert capillary column with a length of 30 m, an internal diameter of 0.25 mm, and a film thickness of 0.25 μm. To identify and quantify the liquid products, an external calibration method was employed. The experiments encompassed five different torrefaction temperatures: 180, 200, 220, 240, and 260 °C, representing a range from light to severe torrefaction. Different durations of 15, 30, and 60 min were considered, while the water/cellulose ratio remained fixed at 10. The selection of a water-to-WCPR ratio of 10 was based on our previous research, where we optimized the water quantity for the WT of WCPR.

The carbon product distribution (selectivity) S(C$_i$) was calculated using the equations below:

$$S(C_i)(mol\%) = \frac{mol(P_i) \times C_n}{\sum mol(P_i) \times C_n} \times 100 \qquad (16)$$

n(P$_i$) and C$_n$ are specified carbon product and carbon number, respectively. The values in this article are in C mol%. The standard deviations of liquid product distribution were determined to be within the range of ± 3.96 % based on a minimum of three experimental repetitions.

3. Results and discussion

3.1. Effect of process parameters on the liquid product distribution of WT + ZSM-5 samples

3.1.1. Effect of reaction time and temperature on the product distribution in the liquid phase of WT + ZSM-5 samples

Fig. 1 exhibits the results of a study the effect of reaction time and temperature on the WT of WCPR with the addition of H-ZSM-5 zeolite catalyst. The focus of the study appears to be on the product distribution in the liquid phase, specifically the conversion of cellulose into various chemical compounds such as ethanol, LA, formic acid, etc. in the presence of different reaction conditions such as reaction time from 15 to 60 min and WT temperature in the range of 180–260 °C. The data highlights a distinct pattern: the formation of ethanol tends to decrease with prolonged reaction time and temperature, while there is an observed increase in the production of LA. This trend suggests that ethanol is an early product, particularly under relatively low WT temperatures, reaching its highest concentration of 89.8 % after just 15 min at 180 °C. Conversely, after a 60 min duration at 240 °C, LA emerges as the primary product, achieving the highest selectivity recorded at 69.5 %.

The product distribution undergoes a significant change with the introduction of the H-ZSM-5 zeolite catalyst. Specifically, it enhances the formation of certain compounds, such as ethanol and LA, while reducing others like 5-hydroxymethylfurfural (5-HMF) and furfural compared to the WT of WCPR without a catalyst, as studied in our previous research work.. The catalyst is likely promoting specific reaction pathways, influencing the selectivity of product formation. In summary, the data suggests that the product distribution in the WT of WCPR is intricately influenced by reaction time, temperature, and the presence of the H-ZSM-5 catalyst.

Fig. 2 shows a valuable comparison of the influence of reaction time, temperature, and the presence of an H-ZSM-5 zeolite catalysts on the production of ethanol, LA and formic acid during the WT of WCPR. It was observed that the ethanol yield decreases consistently with increasing WT temperature across all studied durations (15, 30, and 60 min). For both LA and formic acid production, there is a noticeable increase as the reaction time is extended from 15 to 60 min. This suggests that the torrefaction process is not complete within the initial 15 min and that longer reaction times are necessary for the conversion of WCPR to LA.

The observed maximum in LA at 220 °C after 15 min can be attributed to the optimal temperature for the conversion of WCPR to LA (Fig. 2a). However, as the temperature increases beyond 220 °C, the formation of humins intensifies, leading to a decline in the amount of levulinic acid. This reduction is significant due to the deposition of insoluble humins on the catalyst surface, altering the product distribution and resulting in a decrease in the total soluble products [7]. This phenomenon is well-documented in literature [15], where humins formation not only affects product distribution but also leads to catalyst deactivation. A similar situation is observed with ethanol, where higher temperatures accelerate undesirable reactions, causing a shift in the product distribution. Additionally, Table 1 highlights a notable difference in BET surface area and pore diameter between 220 °C (24.6 m^2/g, 23.5 nm) and 240 °C (14.3 m^2/g, 17.6 nm). This difference can be attributed to the intense formation of humins on the catalyst surface at higher temperatures.

Interestingly, the increase in LA production between 30 and 60 min is particularly pronounced at 260 and 240 °C, indicating that these temperatures are conducive to further conversion of cellulose into LA with extended reaction times. On the contrary, the production of formic acid did not exhibit a strong correlation with reaction time. However, it was noted that the quantity of formic acid increased with a rise in WT temperature within the range of 180–220 °C (15 and 60 min) or 180–240 °C (30 min). Subsequently, as the temperature increased further, the amount of formic acid declined for all WT reaction times.
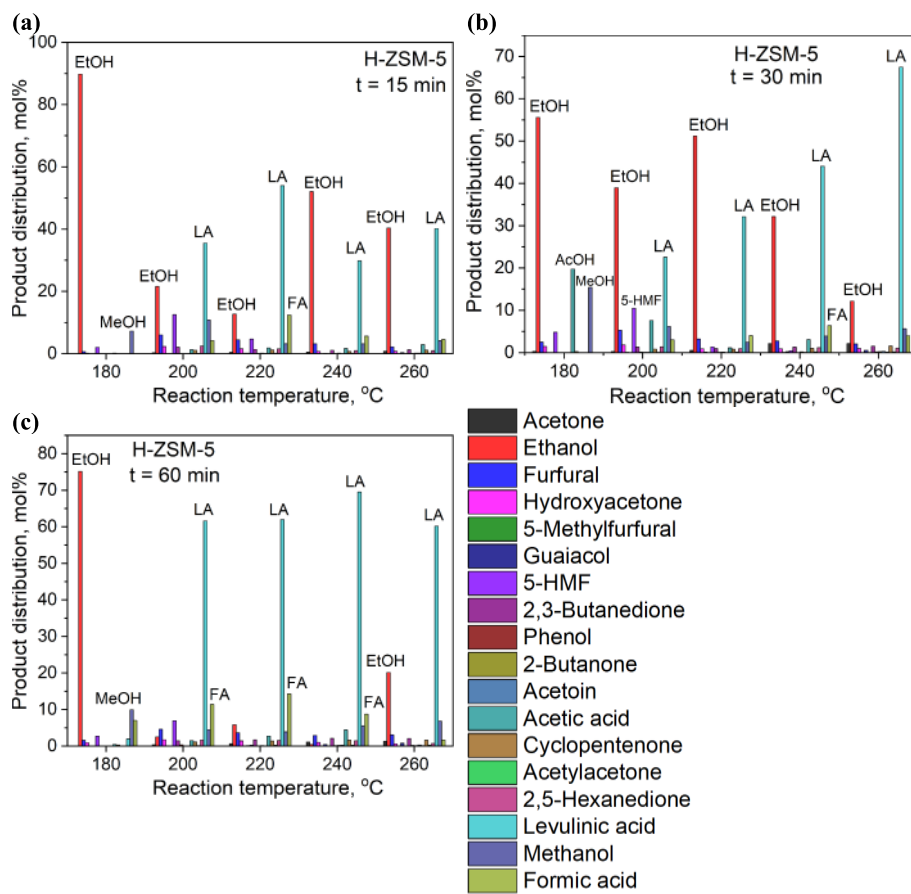
Fig. 1. Effect of reaction time (a – 15 min, b – 30 min, c – 60 min) and temperature on liquid-phase product distribution for the WT + ZSM-5 samples. Reaction conditions: 3.0 g of WCPR, 30 mL of water, 1.0 g of H-ZSM-5 catalyst, stirring speed at 900 rpm, reaction temperature ranging from 180 to 260 °C, and a reaction time of 15 to 60 min.

This phenomenon can be attributed to an increased formation of humins. As illustrated in Fig. 2d, the highest yield for LA (48.2 wt%) was attained at 240 °C after 60 min. Subsequent temperature increases to 260 °C resulted in a reduction in LA yield, attributed to factors such as the formation of by-products (humins), deactivation of some active catalyst sites responsible for LA formation, and a shift in product distribution towards ethanol.

In Fig. 3, it is evident that the liquid product distribution during the wet torrefaction of WCPR, under identical reaction conditions, significantly differs in the absence of a catalyst compared to the distribution observed in the presence of the H-ZSM-5 catalyst (Fig. 1c). In the absence of a catalyst, the primary reaction product for the samples was 5-HMF at 220 °C (Fig. 3a) or acetic acid at 260 °C (Fig. 3b), with selectivities exceeding 60 % and 20 %, respectively. This observation underscores the catalytic effect, as the introduction of a catalyst with acid sites facilitates the conversion of 5-HMF into levulinic acid and formic acid. Conversely, at higher wet torrefaction temperatures without the catalyst, the primary products shift to acetic acid, furfural, and methanol, rather than levulinic acid, highlighting the influence of the catalyst in steering the reaction pathway. This reaction pathway has been experimentally validated and is further expounded upon in the accompanying discussion, elucidating the reaction mechanism as presented in Fig. 11.

Additionally, the results presented in Fig. 4 underscore the significant impact of the H-ZSM-5 catalyst on the wet torrefaction of WCPR under uniform reaction conditions (T = 260 °C, t = 60 min, H₂O/WCPR = 10) compared to WT WCPR without a catalyst. This comparison encompasses key parameters such as HHV, enhancement factor, carbon enrichment, and elemental analysis. The presence of the H-ZSM-5

zeolite catalyst resulted in notable improvements across various metrics. Specifically, HHVs increased from 26.9 to 29.0 MJ/kg, indicating an enhanced energy content. Carbon content exhibited a substantial increase, rising from 67.6 to 76.7 wt%. Furthermore, the enhancement factor experienced a modest increase from 1.40 to 1.44, suggesting a slightly more efficient reaction. Carbon enrichment demonstrated a more pronounced rise, increasing from 1.40 to 1.59, underscoring the positive influence of the catalyst on carbon-based products. These comprehensive findings emphasize the favorable impact of the H-ZSM-5 zeolite catalyst on the specified reaction parameters, highlighting its pivotal role in enhancing both the energy content and structural characteristics of the resulting products.

3.2. TG analysis of WCPR and WT + ZSM-5 samples

The thermogravimetric analysis (TG) was conducted on both WCPR and WT WCPR samples, providing valuable insights into their pyrolysis behavior under various temperature conditions in a nitrogen atmosphere (Fig. 5). These insights significantly contribute to a comprehensive understanding of the thermal stability and decomposition characteristics inherent in these materials. To explore the thermal degradation and combustion behaviours, we examined a temperature range from 50 to 750 °C. Simultaneously, we analyzed samples at 180 and 260 °C after 15 min, and at 220 °C with WT durations of 15, 30, and 60 min. The choice of 220 °C for WT aligns with our previous research, identifying it as the optimal temperature in the absence of a catalyst. Additionally, 180 °C for 15 min was determined as the optimum condition for bio-ethanol production, while 260 °C was chosen for comparison with the sample at 180 °C.
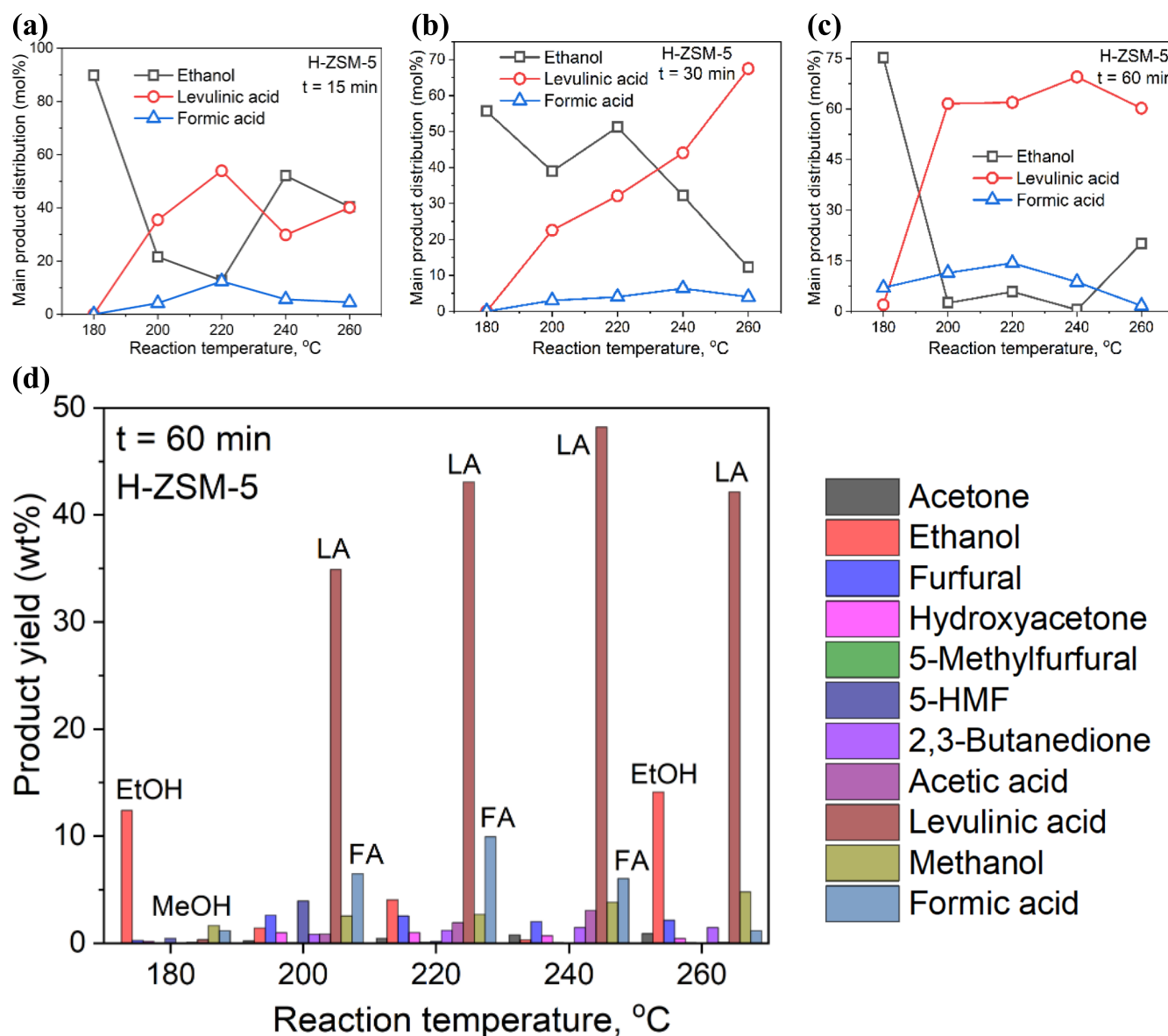
Fig. 2. Effect of reaction time (a) – 15 min, (b) – 30 min, (c) – 60 min, and temperature on the amount of levulinic and formic acids; (d) – effect of reaction temperature on the product yield for the WT + ZSM-5 samples. Reaction conditions: 3.0 g of WCPR, 30 mL of water, 1.0 g of H-ZSM-5 catalyst, stirring speed at 900 rpm, reaction temperature ranging from 180 to 260 °C, and a reaction time of 60 min.

Table 1
Proximate and elemental analysis, BET surface area, pore diameter (PD), crystalline index, and crystallite size of the WT + ZSM-5 samples after 60 min as compared to the WCPR.

Samples	T, °C	Proximate analysis (wt%)				Elemental analysis (wt%)						BET surface area, m^2/g	PD[3], nm	Crystalline index, %
		Moisture	VM[1]	FC[2]	Ash + Si + Al	C	H	O	N	S	Si + Al			
WCPR	–	1.5	75.5	19.8	3.2	48.3	6.2	40.3	0.1	0.5	0	3.4	39.4	76.6
WT + ZSM-5_180	180	3.0	58.9	15.3	22.8	57.3	4.6	31.7	0.1	0.1	6.2	55.8	11.2	75.7
WT + ZSM-5_200	200	5.2	44.1	20.9	29.9	64.8	4.0	22.5	0.1	0.2	8.4	32.4	16.9	66.0
WT + ZSM-5_220	220	2.0	32.1	29.5	36.4	72.6	3.1	19.0	0.1	0.1	5.2	24.6	23.5	36.6
WT + ZSM-5_240	240	3.4	31.0	30.3	35.3	72.1	3.0	18.1	0.1	0.1	6.6	14.3	17.6	25.7
WT + ZSM-5_260	260	4.1	27.9	28.8	39.2	76.7	3.1	12.9	0.1	0.0	7.3	19.3	18.3	30.0

[1] VM – volatile matter, [2]FC – fixed carbon, [3]PD – Average pore diameter measured from the desorption branch according to the BJH method.
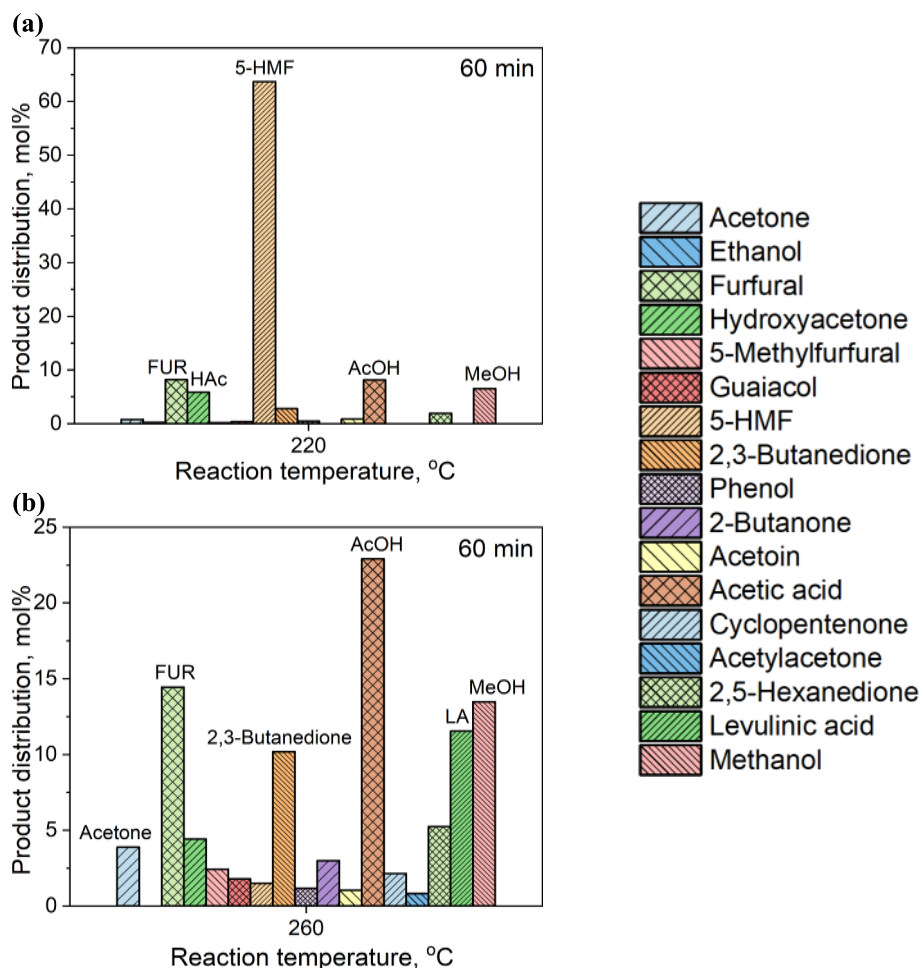
Fig. 3. Liquid product distribution in the absence of ZSM-5 catalyst at different temperatures (a) WT_WCPR_220 at 220 °C, (b) WT_WCPR_260 at 260 °C. Reaction conditions: 3.0 g of WCPR, 30 mL of water, stirring speed at 900 rpm, reaction time of 60 min.

In the TG curves, the residual mass exhibited an increasing trend, rising from 21.2 % to 67.0 % with the elevation of WT temperature. This trend is attributed to a higher proportion of mass in WCPR having been previously lost during the WT process at higher temperatures [37]. Notably, the residual masses of WT_180_15 (37.0 %), WT_220_15 (62.8 %), WT_220_30 (65.1 %), WT_220_60 (64.5 %), and WT_260_15 (67.0 %) were 1.75, 2.96, 3.07, 3.04, and 3.16 times higher than that of the WCPR raw material (21.2 %), respectively. This observation suggests that the thermal stability was enhanced with the escalating WT pre-treatment temperature. TG analysis revealed that WCPR experienced the highest weight loss within the temperature range of 275–350 °C. At the same time, the WT sample at 260 °C (WT_260_15) displayed the highest thermal stability. Remarkably, the WT_260_15 sample not only demonstrated exceptional thermal stability but also exhibited the presence of ethanol and levulinic acid. This observation strongly suggests that WT at this specific temperature setting imparts outstanding thermal resilience to the material while simultaneously promoting the formation of valuable liquid products within the defined parameters of our study. Simultaneously, the sample torrefied at 180 °C (WT_180_15) exhibited the lowest thermal stability (highest weight loss) but still higher than the WCPR feedstock. Notably, the WT_180_15 sample produced the highest yield of bio-ethanol. Furthermore, for the samples torrefied at 220 °C for 15, 30, and 60 min (WT_220_15, WT_220_30, WT_220_60), a correlation was observed wherein thermal stability increased with an extension of WT time.

3.3. HR SEM analysis of WCPR and WT + ZSM-5 samples

The morphology of both the WCPR and the sample obtained through wet torrefaction with and without ZSM-5 catalyst at 260 °C for 60 min was examined using SEM-EDX. The SEM scan images presented in Fig. 6 illustrate notable differences between the WCPR, WT_WCPR, and WT + ZSM-5 samples.

The hydrochar resulting from WT exhibited significant variations in morphology and particle size compared to the untreated WCPR feedstock. While WCPR exhibited a porous structure typical of untreated biomass materials, the cellulose surface underwent a transformative process after WT in the presence of the H-ZSM-5 catalyst (Fig. 6c). This transformation resulted in a flatter and smoother texture with some grooves, yet it retained elements of the original fiber morphology. This notable change in morphology is attributed to the thermochemical reactions occurring during the WT process. Additionally, the surface area and pore characteristics were detailed in Table 1. Evidently, wet torrefaction treatment improved the surface area of the hydrochar, albeit with a simultaneous reduction in pore diameter. Moreover, the presence of H-ZSM-5 particles was identified on the WT samples (Fig. 6c). The H-ZSM-5 zeolite catalyst plays a crucial role in facilitating the WT process, likely by promoting the formation of intermediates and selectively catalysing specific reactions, leading to the production of ethanol and/or LA and other valuable products. The acidic and porous nature of the H-ZSM-5 zeolite provides an ideal environment for catalytic reactions, enabling the effective conversion of cellulose into valuable chemicals.

The surface of the WT_WCPR sample (Fig. 6b) undergoes a noticeable
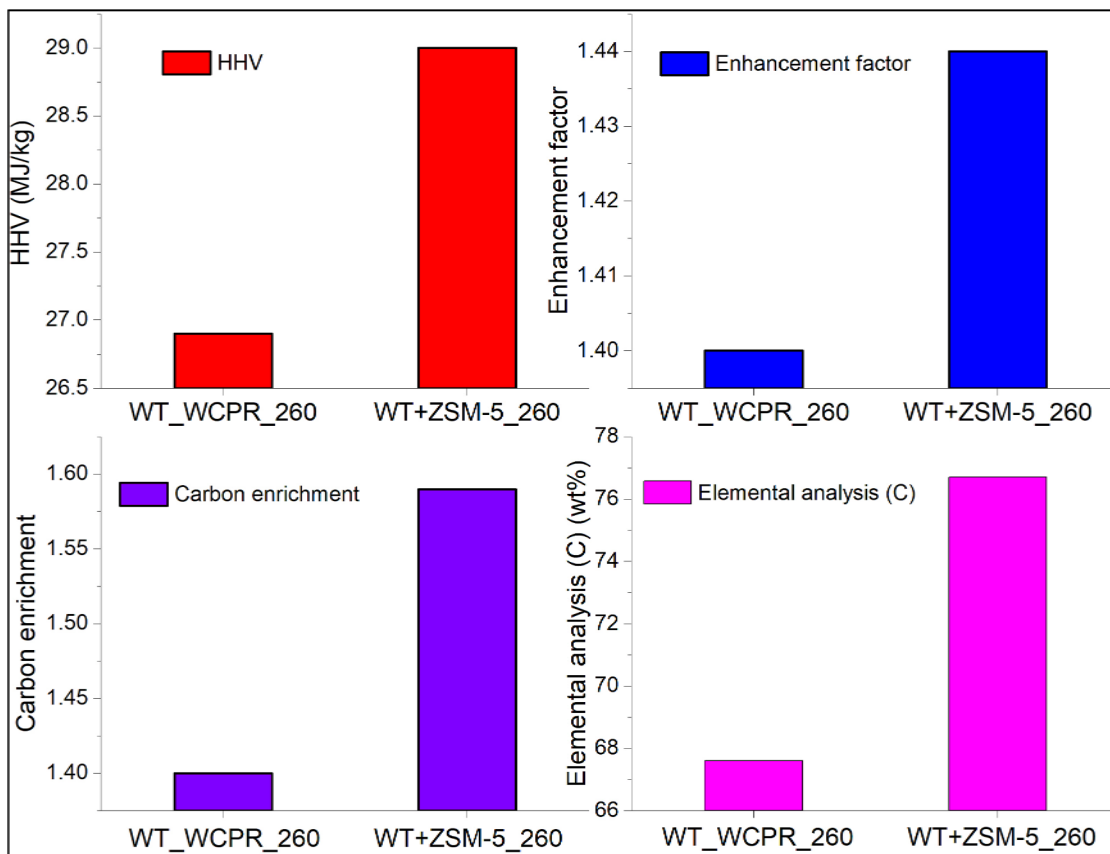
Fig. 4. Comparative analysis of HHV, enhancement factor, carbon enrichment, and elemental analysis (C) in the presence and absence of H-ZSM-5 catalyst at 260 °C. Reaction conditions: 3.0 g of WCPR, 30 mL of water, stirring speed at 900 rpm, reaction time of 60 min.
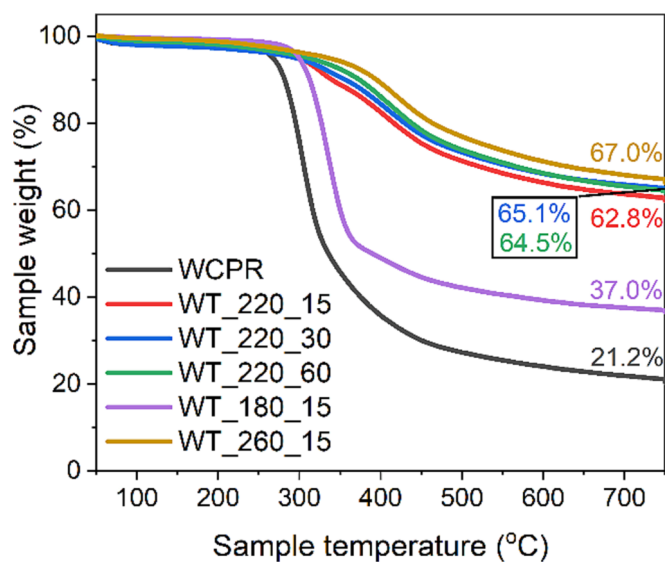
Fig. 5. TG curves for WCPR and WT WCPR samples with 1.0 g of H-ZSM-5 catalyst within 15–60 min at 180, 220 and 260 °C at the heating rate of 10 °C/min in nitrogen atmosphere.

transformation, exhibiting a flatter and smoother texture when compared to the original WCPR feedstock. This alteration in morphology is likely a result of the thermochemical reactions taking place during the WT process.

The SEM-EDX analysis offers valuable insights into the elemental composition of the WCPR raw material and the alterations that take place following WT, both in the presence and absence of the H-ZSM-5 catalyst (Table S4). The carbon content in the dried cellulose ranges from 57.97 to 58.57 %, which is expected for cellulose, primarily composed of carbon. Following WT, the carbon content decreases significantly, ranging from 45.68 to 45.26 %. This reduction in carbon indicates that the torrefaction process caused the breakdown of carbon-rich cellulose molecules, leading to the release of volatile components and the conversion of cellulose into other products, such as LA and other degradation byproducts. Surprisingly, the oxygen content in the wet torrefied sample ranges from 42.01 to 43.95 %, showing a slight increase after torrefaction. This could be attributed to the loading of zeolite, including SiO_2 and Al_2O_3, as confirmed by the detected amount of Si (10.65–11.68 %) in the torrefied sample with the catalyst.

Silicon is detected in trace amounts in the feedstock, and its presence becomes more pronounced in the wet torrefied sample, along with the appearance of aluminum. These elements are likely attributed to the introduction of the H-ZSM-5 catalyst during the torrefaction process. On the other hand, calcium is detected in trace amounts in the feedstock and remains at low levels in the wet torrefied sample, possibly originating from impurities in the biomass or catalyst.

Following WT at 220 °C for 30 min without presence of catalyst, Si, S, and Ca were undetectable in the treated samples. The primary alterations observed included a marginal rise in carbon content and a minor reduction in oxygen content after WT of WCPR. Despite these changes being relatively modest, the overall composition appears to maintain a similarity to the original feedstock.

3.4. XRD analysis of WCPR and WT + ZSM-5 samples

The X-ray diffraction (XRD) patterns obtained for both the WCPR and the corresponding WT + ZSM-5 samples (Fig. 7) revealed distinct peaks
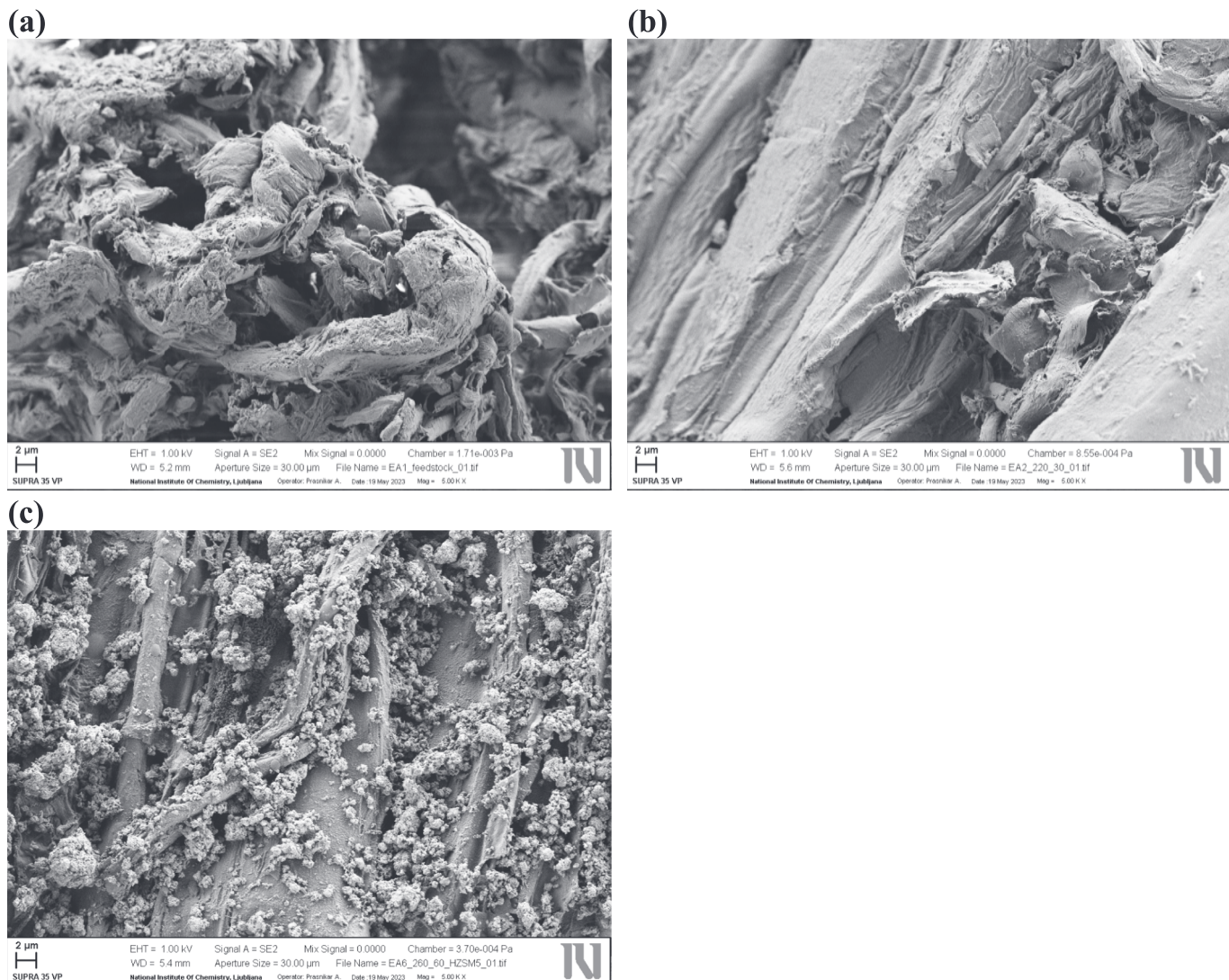
Fig. 6. SEM scans of WCPR – (a), WT_WCPR – (b), and WT + ZSM-5 sample – (c).
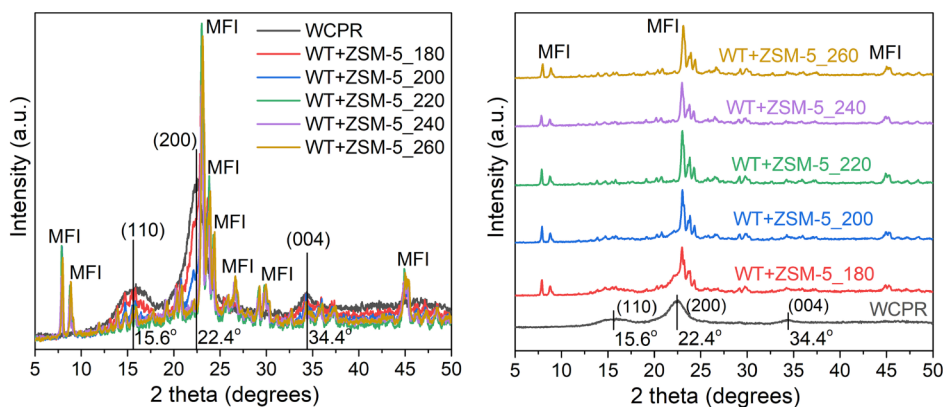
Fig. 7. X-ray diffraction pattern of the wet torrefied samples with H-ZSM-5 zeolite at 180–260 °C ("WT + ZSM-5_180" – "WT + ZSM-5_260") as compared to the WCPR.

at 2θ values of 15.6, 22.4, and 34.4°. These peaks were identified as the crystalline planes indexed as (1 1 0), (2 0 0), and (0 0 4), respectively, within the cellulose type I allomorph's crystal structure. It is essential to highlight that cellulose is the only component exhibiting a crystalline structure, whereas hemicellulose and lignin display amorphous characteristics [38]. These findings highlight a significant alteration in the crystalline integrity of cellulose during the WT process. This transformation includes modifications in the polymorphic structure of cellulose I, resulting in a noticeable decrease in its crystallinity and, in some cases, the eventual disappearance of characteristic peaks.

Simultaneously, the XRD pattern of the H-ZSM-5 zeolite catalyst, associated with MFI topology (JCPDS 42–0024), exhibited a high degree of crystallinity and strong intensity diffraction peaks in the 2θ region of 20–25° at 23.1, 23.3, 23.7, 23.9, 24.4°, and in the 2θ region of 7–10° at 7.9, 8.8, and 9.1° [39]. Notably, the most prominent characteristic peaks for the MFI framework were identified in the WT + ZSM-5_220 and WT + ZSM-5_260 samples.

3.5. Elemental components and surface properties of WCPR and WT + ZSM-5 samples

Table 1 shows the proximate analysis data, offering valuable insights into the compositional changes of WCPR during WT at different temperatures in the presence of ZSM-5 zeolite catalyst. The volatile matter content undergoes a notable decline as the torrefaction temperature rises. Starting at 58.9 % for WT + ZSM-5_180, it decreases consistently to 27.9 % for the WT + ZSM-5_260 sample. This reduction signifies the release of volatile organic compounds as the WCPR undergoes thermal treatment. The fixed carbon content exhibits a distinctive pattern during torrefaction. It decreases from 19.8 % (for untreated WCPR) to 15.3 % at 180 °C. However, beyond 200 °C, there is a subsequent increase in fixed carbon content, reaching 30.3 % at 240 °C. This trend suggests a complex interplay between the degradation and stabilization of carbonaceous components during torrefaction. The combined percentage of ash, silicon, and aluminum (Ash + Si + Al) reveals interesting trends in residue/mineral composition. Starting at 22.8 % for WT + ZSM-5_180, it steadily increases with temperature, reaching 39.2 % for WT + ZSM-5_260. This rise could be attributed to the concentration effect as volatile components are released, leaving behind a higher coke formation and thus proportion of ash.

The elemental analysis data in Table 1 and Fig. 10b provides a quantitative understanding of the compositional changes in WCPR during WT with ZSM-5 zeolite catalyst at different reaction temperatures. Starting with WCPR, the carbon content increases from 48.3 to 76.7 % in WT + ZSM-5_260, indicating a significant enrichment in carbonaceous material. The hydrogen content exhibits a decline, decreasing from 6.2 % in WCPR to 3.0 % in the case of the WT + ZSM-5_240 sample. The reduction in oxygen content is evident as torrefaction temperature increases. WCPR, with an oxygen content of 40.3 %, undergoes a decrease to 12.9 % in WT + ZSM-5_260. This decline aligns with the removal of oxygenated functional groups, indicative of biomass waste transformation and improved fuel properties. Nitrogen and sulfur remain at minimal levels across all samples. WCPR starts with 0.1 % nitrogen and 0.5 % sulfur, and these values remain consistently low in subsequent samples. The Si + Al content exhibits variation, showing an increase from 0 % in WCPR to 5.2–8.4 % in the WT + ZSM-5 samples. The presence of Si and Al can be attributed to the utilization of the H-ZSM-5 catalyst compared to the WCPR feedstock alone. Discrepancies in the amounts of Si and Al among samples could potentially be attributed to experimental errors and the non-homogeneous distribution of zeolite on wet torrefied material.

The structural and morphological characteristics of the studied samples were studied (Table 1). The parameters under investigation include temperature BET surface area (m^2/g), average pore diameter (PD, nm), crystalline index (%), and crystallite size (nm). The BET surface area is a key parameter influencing the adsorption and catalytic properties of materials. It is observed that the WT + ZSM-5_180 sample exhibits the highest BET surface area (55.8 m^2/g) among the samples, indicating a substantial surface available for catalytic activities.

Conversely, the WCPR feedstock shows the lowest surface area (3.4 m^2/g), suggesting differences in the porous structure between wet torrefied and untorrefied materials. The average pore diameter, as determined by the BJH method, provides insights into the pore size distribution. The WCPR feedstock has a relatively larger average pore diameter (39.4 nm) compared to lowest pore diameter (11.2 nm) of the WT + ZSM-5_180 sample. This disparity in pore diameter may influence

the diffusion and accessibility of reactants within the materials, impacting their catalytic performance. Remarkably, the WT + ZSM-5_180 sample exhibits the highest ethanol yield, accompanied by both the greatest surface area and the smallest pore diameter when compared to the other samples studied.

The crystalline index serves as an indicator of the degree of crystallinity within the samples. Notably, in the absence of a catalyst, the WT samples within the temperature range of 180–220 °C exhibit elevated crystalline indices (78.0 %, 76.4 %, and 74.4 %, respectively) in comparison to those at 240 and 260 °C. This discrepancy implies that the latter two samples may possess a more amorphous and/or disordered structure, particularly as the WT temperature exceeds 220 °C.

Conversely, the introduction of ZSM-5 results in a decline in the crystallinity index. The reduction becomes apparent at 200 °C, where the index decreases to 66.0 %, and further drops significantly to 36.6 % at 220 °C, when compared to WT samples without the catalyst. Notably, at 240 °C, the crystallinity indices of both samples (with and without catalyst) align with each other. This discrepancy between wet torrefied samples with and without catalyst can be elucidated by the increased reactivity of WCPR in the presence of ZSM-5 catalyst. This catalytic synergy leads to the production of a more amorphous solid material (hydrochar) under identical WT conditions.

Crystallite size is a critical parameter influencing the catalytic activity of materials. The crystallite size data indicates subtle variations among the samples, ranging from 0.8 to 3.6 nm. Interestingly, the WT samples 240 and 260 °C show significantly smaller crystallite sizes (0.8 nm) compared to the other samples. The smaller crystallite sizes in certain samples may contribute to enhanced reactivity, particularly at higher temperatures.

3.6. HHV, solid, carbon, hydrogen, energy yields, DC, DH, DO, enhancement factor, carbon enrichment, weight loss and atomic ratios of O/C and H/C of WCPR and WT + ZSM-5 samples

This research extensively investigates the higher heating values (HHVs) associated with untreated WCPR and WT + ZSM-5 samples. The HHVs of the hydrochar products exhibit a clear dependence on the WT temperature. As the temperature increases from 180 to 260 °C, a discernible trend in HHV is observed, indicating the significance of temperature in influencing the energy content of the resulting hydrochar (Table 2 and Fig. 8a). The HHV of WCPR (20.1 MJ/kg) is surpassed by all WT + ZSM-5 samples. Analysis of the data reveals that the WT + ZSM-5_260 sample has the highest HHV (29.0 MJ/kg) among all tested temperatures. This implies that 260 °C is the optimal temperature for WT when seeking to maximize the higher heating value of the resulting hydrochar.

Energy yield provides a quantitative measure of the effectiveness of a system or process, reflecting the percentage of energy extracted or generated compared to the total available energy in the input material. At 180 °C, the energy yield is notably high at 92.0 %. This suggests that the addition of H-ZSM-5 zeolite at this temperature significantly enhances the WT process, leading to a substantial increase in energy yield. At 200 °C, there is a significant decrease in energy yield to 53.8 %. This decline might be attributed to changes in the torrefaction kinetics or the onset of undesired side reactions at higher temperatures, despite the catalytic influence. The constant energy yield at 40.9 % for both 220 and 240 °C indicates a potential temperature range where the catalytic WT process reaches a stable efficiency, suggesting that the catalysis has a consistent impact within this temperature window. At 260 °C, there is a slight increase in energy yield to 43.3 %, indicating that the catalytic system may still exert influence at higher temperatures, albeit with a more modest improvement.

Table 2 presents the carbon and hydrogen yield data, revealing notable results at 180 °C with a significant carbon yield of 99.0 % and a corresponding hydrogen yield of 62.1 %. This observation suggests that, in the early stages of WT, there is minimal removal of carbon, with

Table 2
HHV, solid yield, carbon yield, hydrogen yield, energy yield, DC, DH, DO, EF, atomic ratios, CE and WL of the WT + ZSM-5 samples after 60 min as compared to the WCPR.

Samples	T, °C	H₂O/ WCPR ratio	HHV, MJ/ kg	Solid yield, wt %	Carbon yield, wt%	Hydrogen yield, wt%	Energy yield, %	DC[1], wt%	DH[2], wt%	DO[3], wt%	EF[4]	Atomic ratio		CE[5]	WL[6], wt%
												O/ C	H/ C		
WCPR	–	–	20.1	–	–	–	–	–	–	–	1.00	0.6	1.5	1.00	–
WT + ZSM-5_180	180	10	22.2	83.5	99.0	62.1	92.0	1.0	31.6	27.6	1.10	0.4	1.0	1.19	16.5
WT + ZSM-5_200	200	10	25.0	43.3	58.1	27.7	53.8	41.9	65.6	69.9	1.24	0.3	0.7	1.34	56.7
WT + ZSM-5_220	220	10	27.0	30.5	45.8	15.0	40.9	54.2	79.9	80.8	1.34	0.2	0.5	1.50	69.5
WT + ZSM-5_240	240	10	26.8	30.7	45.7	14.9	40.9	54.3	80.1	81.6	1.34	0.2	0.5	1.49	69.3
WT + ZSM-5_260	260	10	29.0	30.0	47.6	14.8	43.3	52.4	78.6	86.2	1.44	0.1	0.5	1.59	70.0

[1] DC – decarbonization, [2]DH – dehydrogenation, [3]DO – deoxygenation, [4]EF – enhancement factor, [5]CE – carbon enrichment, [6]WL – weight loss (conversion).
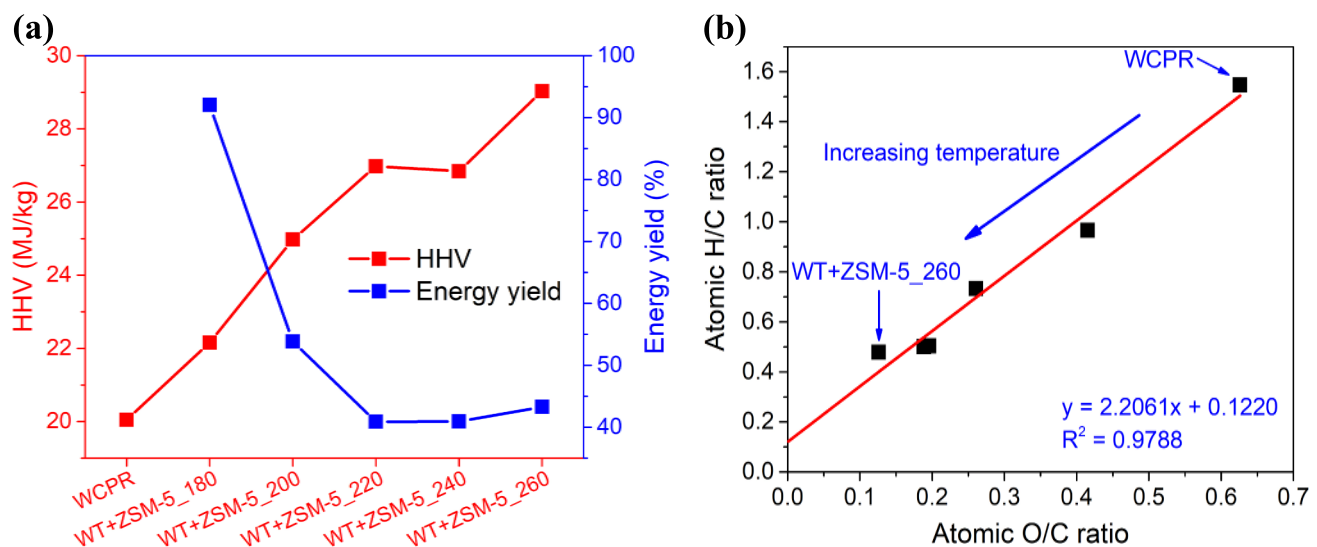
Fig. 8. HHV and energy yield – (a) and H/C versus O/C ratio in terms of atomic basis (van Krevelen diagram) – (b) for WCPR and WT + ZSM-5 samples.

dehydration emerging as the primary reaction mechanism responsible for hydrogen removal at the initiation of the process. However, at 200 °C, both carbon and hydrogen yields experience a decrease, a trend attributed to the substantial removal of volatile components during the WT process. Remarkably, at 220 and 240 °C, the yields stabilize, indicating a potential temperature plateau in the torrefaction process. At 260 °C, a slight increase in carbon yield hints at continued torrefaction activity, while hydrogen yield remains stable.

The van Krevelen diagram, depicted in Fig. 8b, reveals the atomic H/C and atomic O/C ratios. This diagram unveils a relatively strong linear correlation (R^2 = 0.9788) wherein both H/C and O/C ratios decrease with increasing temperatures under an N_2 atmosphere. The observed reduction in H/C and O/C ratios in the van Krevelen diagram signifies enhanced carbonization [40]. This decrease in ratios suggests an improvement in the carbonization process as temperatures rise, indicating a crucial correlation between temperature and the efficiency of carbonization.

The enhancement factors exhibit a clear ascending trend, with values increasing from 1.10 at 180 °C to 1.44 at 260 °C. This progression signifies an augmented efficiency in WCPR conversion with higher temperatures, suggesting an intensified transformation of the raw material into more energy-dense products. Concurrent with the enhancement factors, carbon enrichment values also demonstrate a consistent rise from 1.19 at 180 °C to 1.59 at 260 °C. The substantial increase in weight

loss percentages is noteworthy, starting at 16.5 % at 180 °C and reaching 70.0 % at 260 °C. This signifies a temperature-dependent removal of volatile components during torrefaction, contributing to the enrichment of carbon in the solid residue.

In Fig. 9, the graphs depict enhancement factor profiles in relation to the atomic O/C ratio and carbon enrichment for both WCPR and WT + ZSM-5 samples.

Noteworthy is the strong linear trend observed in both correlations, with the atomic O/C ratio (R^2 = 0.9508) and carbon enrichment (R^2 = 0.9883) exhibiting a significant association. An elevation in carbon enrichment is associated with a higher enhancement factor, while an increase in the O/C ratio is conversely linked to a lower enhancement factor.

Table 2 and Fig. 10 present comprehensive data on decarbonization (DC), dehydrogenation (DH), and deoxygenation (DO) for various samples, encompassing elemental analysis of WCPR and WT + ZSM-5 samples at different reaction temperatures. The elemental removal sequence during WT, with DO > DH > DC (excluding WT + ZSM-5_180), underscores the substantial impact of torrefaction on reducing oxygen content compared to other elements [41]. DC quantifies the reduction in carbon content in WCPR during the WT process, revealing a gradual increase in DC with escalating treatment severity. For example, the DC rate in the WT + ZSM-5_180 (1.0 %) sample is low but experiences a noteworthy increase in the WT + ZSM-5_200 (41.9 %) sample.
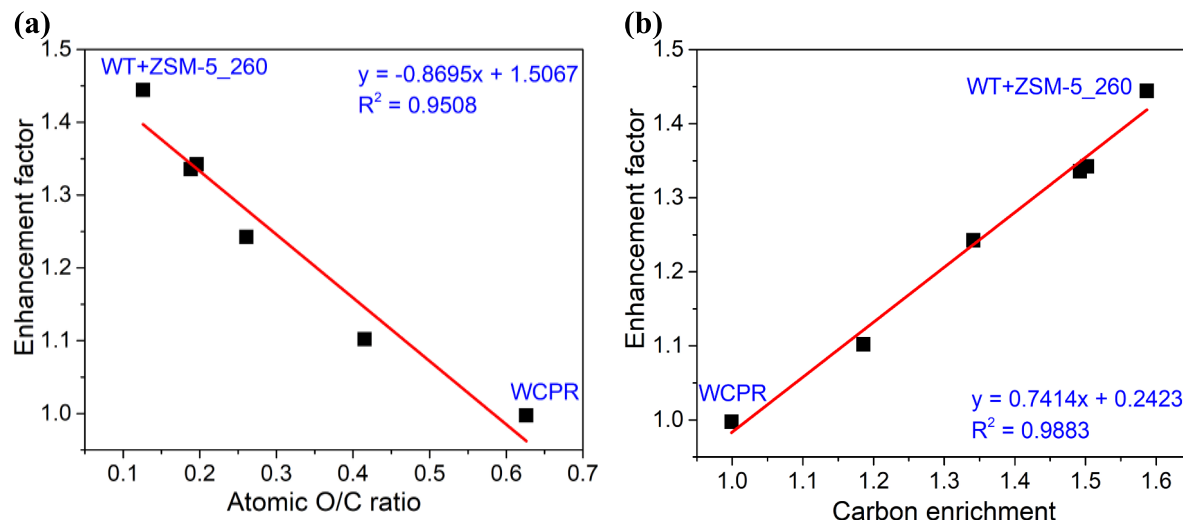
Fig. 9. Enhancement factor versus O/C ratio – (a) and carbon enrichment – (b) for WCPR and WT + ZSM-5 samples.
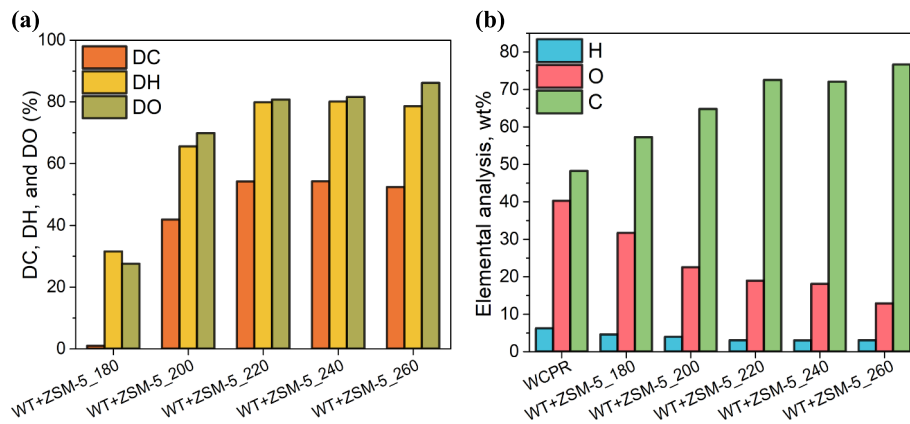
Fig. 10. (a) – profiles of decarbonization (DC), dehydrogenfation (DH), and deoxygenation (DO) and (b) – elemental analysis (H, O, C) of WCPR and WT + ZSM-5 samples in the temperature range of 180–260 °C.

A similar pattern is notably observed in DH and DO, with a more pronounced increase, reaching 80.1 % and 86.2 %, respectively. This consistent trend indicates that as the severity of WT conditions intensifies, there is a substantial removal of oxygen, hydrogen, and carbon from the WCPR. This outcome is of significant importance as it contributes to a reduction in carbon content and enhances the C/H and C/O ratios in the resulting hydrochar. These transformations render the hydrochar more suitable as a solid fuel source, exhibiting improved fuel characteristics suitable for a diverse range of applications.

To deepen the discussion and enhance the comparison with other researchers' results, we conducted a comprehensive data analysis. The findings are presented in Table 3, which compares the HHV and ultimate composition of biochar from various biomass types following wet torrefaction under optimal reaction conditions. Table 3 highlights that the WT + ZSM-5_260 sample demonstrates the highest HHV (29.0 MJ/kg) and carbon content (76.7 wt%) in biochar compared to a range of biomass types, including bamboo sawdust [42,43], rice husk [44], corn stalk [45], beech [46], wheat straw [46,47], spruce [48], birch [48], oil trimmings and pulp [49], eucalyptus bark [50], palm oil empty fruit bunches [51], grape pomace [52], and dried olive pomace [53].

Across all biomass types, there is a general increase in HHV with temperature, and HHV strongly correlates with the biomass's carbon, hydrogen, oxygen, and nitrogen contents. Despite our wet torrefaction temperature not being the highest compared to certain studies (e.g., [50–52]), where temperatures reached 300 °C, 350 °C, and 275 °C,

respectively, our HHV and carbon content surpass theirs, while maintaining the lowest oxygen content (12.9 wt%). We attribute this enhancement in HHV of wet torrefied WCPR to the concentrated carbon content and decreased oxygen content resulting from more intense dehydration reactions in the presence of the H-ZSM-5 catalyst compared to biomass feedstock from literature where the catalyst was not present. We further suggest that the reduction in oxygen content primarily arises from the degradation of cellulose due to the reaction with the acidic H-ZSM-5 zeolite catalyst, given its oxygen-rich nature relative to lignin [28]. This phenomenon also contributes to the decreased solid yield with increasing temperature (Table 2).

Thus, the careful selection of the temperature range for WT of lignocellulosic biomass is crucial, considering the diverse properties of different biomass sources to ensure efficient production and cost-effectiveness. With ongoing improvements in catalyst efficiency, selectivity and heightened robustness, the one-pot chemocatalytic approach is positioned to demonstrate significant potential for the practical production of high-quality biochar, bio-ethanol, and levulinic acid products from biomass waste in the future.

3.7. Reaction pathways of WCPR into hydrochar and the liquid products

Ethanol, levulinic acid, and biochar are produced simultaneously during the wet torrefaction process of WCPR. However, the quantities and qualities of each product vary depending on the specific reaction

Table 3

Comparison of higher heating value (HHV) and ultimate composition of biochar from different precursor biomass types following wet torrefaction under optimal reaction conditions.

Biomass	T, °C	Time, min	Biomass-to-liquid ratio, g:g	HHV, MJ/kg	Ultimate analysis (wt%)					Ref.
					C	H	O	N	S	
Bamboo sawdust	–	–	–	17.7	49.2	6.6	43.1	0.4		[42]
	230	30	1:10	20.8	53.4	6.2	40.2	0.1		
Rice husk	–	–	–	16.2	40.8	5.7	40.5	1.2	–	[44]
	240	60	1:20	18.1	45.8	5.2	33.1	0.4	–	
Corn stalk	–	–	–	17.7	44.5	6.3	46.4	0.3	–	[45]
	220	30	1:15	21.2	53.3	6.0	40.0	0.4	–	
Bamboo sawdust	–	–	–	17.7	49.2	6.6	43.1	0.4	–	[43]
	240	30	1:10	20.9	64.8	4.4	30.3	0.2	–	
Beech	–	–	–	17.4	44.9	5.0	40.9	0.1	0.04	[46]
	200	10	1:20	19.1	48.9	5.4	40.9	0.2	0.03	
Wheat straw	–	–	–	17.1	45.0	4.6	37.6	0.6	0.1	
	200	10	1:20	19.3	49.7	5.0	38.4	0.6	0.1	
Spruce	–	–	–	20.4	50.3	6.2	43.4	0.1	<0.02	[48]
	225	30	1:5	23.0	57.0	5.9	37.1	0.1	<0.02	
Birch	–	–	–	20.0	48.9	6.4	44.6	0.1	<0.02	
	225	30	1:5	22.9	56.9	5.9	42.6	0.1	<0.02	
Olive trimmings	–	–	–	19.8	48.3	6.1	40.0	1.5	–	[49]
	250	30	1:10	27.2	60.3	6.3	28.2	1.8	–	
Olive pulp	–	–	–	21.7	50.3	5.8	39.2	1.6	–	
	250	30	1:10	27.6	62.9	6.3	24.8	1.7	–	
Eucalyptus bark	–	–	–	18.1	45.2	6.4	48.4	–	–	[50]
	300	120	1:10	28.9	72.7	5.1	22.2	–	–	
Palm oil empty fruit bunches	–	–	–	19.5	48.3	6.7	43.7	1.0	0.3	[51]
	350	30	1:6.7	27.2	66.0	4.2	28.4	1.1	0.3	
Grape pomace	–	–	–	20.0	49.1	6.3	42.3	2.3	–	[52]
	275	30	1:4	28.3	68.3	5.9	23.5	2.3	–	
Wheat straw	–	–	–	17.6	45.0	5.7	44.6	0.4	0.4	[47]
	240	60	1:10	23.9	60.7	5.6	29.5	0.6	0.4	
Dried olive pomace	–	–	–	22.5	53.5	6.8	38.6	1.1	–	[53]
	250	30	1:6	27.6	67.8	6.5	24.3	1.4	–	
WCPR	–	–	–	20.1	48.3	6.2	40.3	0.1	0.5	This study
WT + ZSM-5	260	60	1:10	29.0	76.7	3.1	12.9	0.1	–	

conditions. We postulate that the WT of WCPR, in the presence of H-ZSM-5 zeolite catalyst in an N_2 atmosphere (Fig. 11), involves two primary pathways leading to ethanol production. The first and main pathway involves the direct conversion of cellulose into hydroxyacetone, followed by the subsequent formation of ethanol through C–C cleavage of hydroxyacetone. This route necessitates the activation and cleavage of specific C–C and C–O bonds. While recent literature [15,18–20,54–56] has demonstrated the direct generation of ethanol from cellulose using different heterogeneous catalysts involving glycolaldehyde transformation into ethylene glycol and promoting the C–O cleavage of ethylene glycol to yield ethanol, our study has identified diverse reaction products. Consequently, we propose an alternative reaction mechanism based on the observed hydroxyacetone product. In addition to ethanol resulting from the C–C cleavage of hydroxyacetone, our study detected byproducts such as methanol and acetaldehyde. Furthermore, an additional quantity of ethanol can be obtained through acetaldehyde transfer hydrogenation, while acetic acid is produced through the oxidation of acetaldehyde. Finally, a minor amount of formaldehyde and CO_2 was detected, likely arising from the hydroxyacetone cracking process.

The second pathway encompasses a series of distinct steps. The process begins with cellulose hydrolysis into glucose, catalyzed by the acid centers of H-ZSM-5 zeolite, particularly Lewis and Brønsted acid sites (LASs and BASs) [56–58]. Following hydrolysis, glucose undergoes isomerization into fructose over LASs [55], and subsequently, fructose undergoes a sequential transformation into hydroxyacetone through retro aldol-condensation. Finally, hydroxyacetone is converted into ethanol through C–C cleavage. Concurrently, we acknowledge the potential conversion of glucose to hydroxyacetone *via* retro aldol-condensation as well.

The synthesis of LA from cellulose derived from lignocellulosic biomass involves a multi-step process. Initially, cellulose undergoes

hydrolysis to form glucose, which is then converted to 5-HMF. The subsequent transformation of 5-HMF into LA constitutes the final stage [59]. In the first step, glucose resulting from cellulose hydrolysis undergoes dehydration, leading to the formation of 5-HMF, with active participation of LASs. Following this, 5-HMF is rehydrated into LA, the primary target compound, accompanied by the concurrent generation of formic acid. This transformative process is facilitated by BASs, contributing to the cleavage of C–C bonds. Moreover, it is known [60,61] that in acidic solutions, the direct dehydration of glucose without the intermediate formation of fructose and 5-HMF is a plausible process.

Simultaneously, glucose can undergo isomerization with the participation of LASs to yield fructose. Subsequently, fructose undergoes a dehydration reaction, leading to the formation of 5-HMF with the involvement of BASs [58,62]. The rehydration of 5-HMF results in the production of LA and formic acid. Additionally, within the product mixture, furfural may be generated due to the release of formaldehyde from the 5-HMF compound [60,62]. Notably, the observed formation of humins aligns with existing literature [23,63], suggesting that under acid catalysis, glucose polymerization and 5-HMF can produce humins through aldol condensation with an intermediate compound, 2,5-dioxo-6-hydroxyhexanal.

4. Conclusions

In this study, we introduce a novel chemocatalytic approach for the one-pot production of levulinic acid (LA) and/or ethanol during wet torrefaction (WT) of wood cellulose pulp residue (WCPR) in a presence of H-ZSM-5 zeolite catalyst, concurrently yielding high-quality solid fuel. We systematically explored the impact of acid catalyst and varied reaction conditions on hydrochar properties and liquid product distribution. The study underscores the significant influence of WT
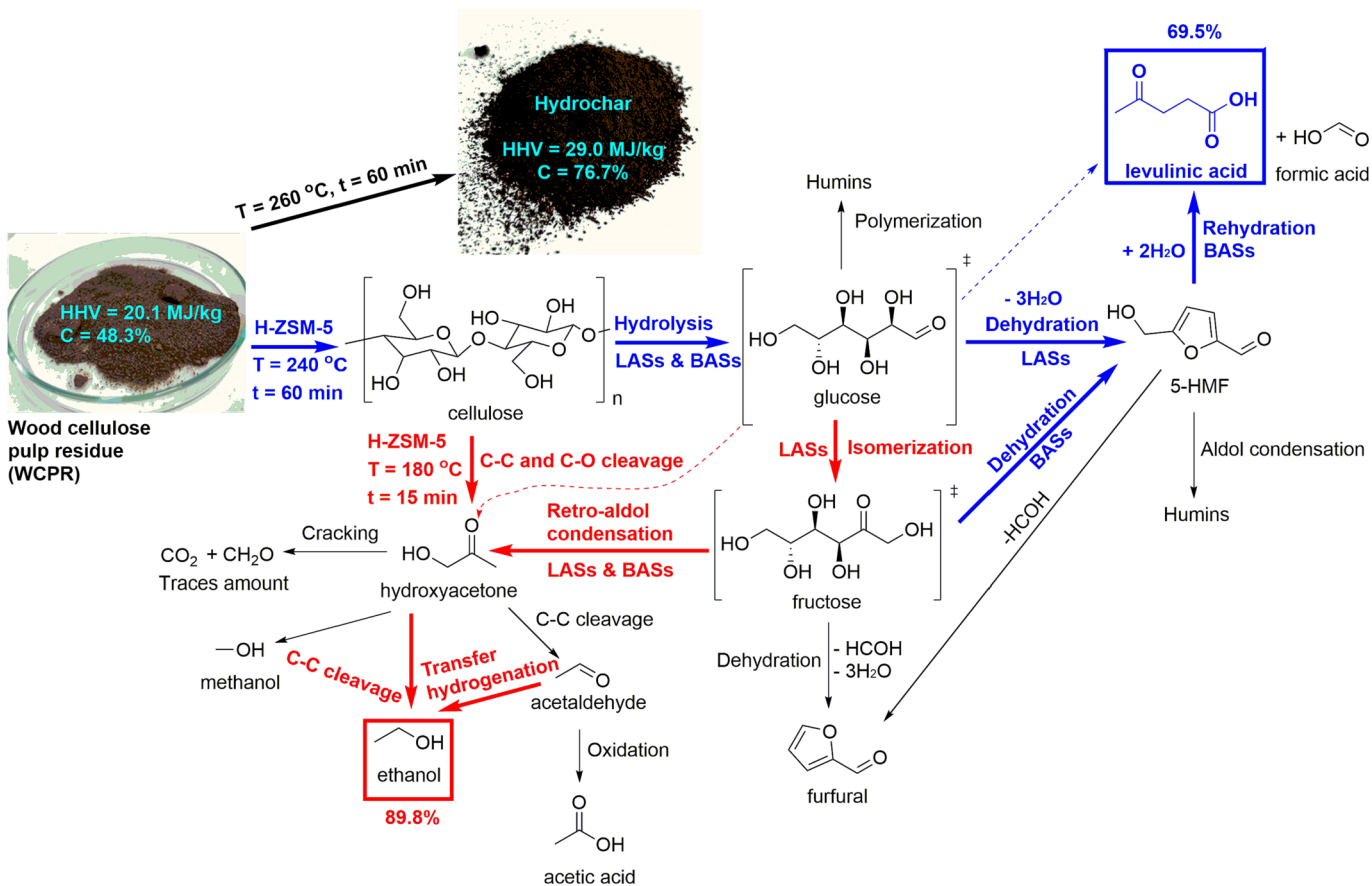
Fig. 11. Possible reaction mechanism for the WT of WCPR with H-ZSM-5 zeolite catalyst into hydrochar and the liquid value-added products such ethanol and levulinic acid.

conditions, particularly WCPR with H-ZSM-5 zeolite catalyst, on hydrochar characteristics and liquid product distribution. Detailed analyses reveal substantial alterations in hydrochar composition with elevated temperatures and durations. Optimal conditions for bioethanol production were identified at 180 °C for 15 min, resulting in a remarkable selectivity of 89.8 %. Similarly, optimal conditions for LA production were found at 240 °C for 60 min, yielding a selectivity of 69.5 %. Additionally, an extensive assessment of various hydrochar properties was conducted, encompassing higher heating values (HHVs), decarbonization, dehydrogenation, deoxygenation, enhancement factor, carbon enrichment, surface area, pore diameter, and yields. The highest carbon content, reaching 76.7 %, was attained at 260 °C after a 60 min treatment, resulting in an HHV of 29.0 MJ/kg, an enhancement factor of 1.44, and carbon enrichment of 1.59. Furthermore, our comprehensive reaction mechanism elucidates the WT of WCPR with the H-ZSM-5 zeolite catalyst under optimized conditions. This study highlights the potential of WT as a valuable process for converting WCPR into sustainable energy (high-quality hydrochar) and chemicals (ethanol and LA).

CRediT authorship contribution statement

Andrii Kostyniuk: Writing – review & editing, Writing – original draft, Visualization, Validation, Software, Resources, Project administration, Methodology, Investigation, Formal analysis, Data curation, Conceptualization. **Blaž Likozar:** Supervision, Project administration, Funding acquisition, Conceptualization.

Declaration of competing interest

The authors declare that they have no known competing financial interests or personal relationships that could have appeared to influence the work reported in this paper.

Data availability

Data will be made available on request.

Appendix A. Supplementary data

Supplementary data to this article can be found online at https://doi.

org/10.1016/j.cej.2024.149779.

References

[1] O. Ali Qamar, F. Jamil, M. Hussain, A.H. Al-Muhtaseb, A. Inayat, A. Waris, P. Akhter, Y.K. Park, Feasibility-to-applications of value-added products from biomass: current trends, challenges, and prospects, Chem. Eng. J. 454 (2023) 140240, https://doi.org/10.1016/j.cej.2022.140240.

[2] S. Fakudze, J. Chen, A critical review on co-hydrothermal carbonization of biomass and fossil-based feedstocks for cleaner solid fuel production: synergistic effects and environmental benefits, Chem. Eng. J. 457 (2023) 141004, https://doi.org/10.1016/j.cej.2022.141004.

[3] N. Saha, E. Fillerup, B. Thomas, C. Pilgrim, T. Causer, D. Herren, J. Klinger, Improving bamboo's fuel and storage properties with a net energy export through torrefaction paired with catalytic oxidation, Chem. Eng. J. 440 (2022) 135750, https://doi.org/10.1016/j.cej.2022.135750.

[4] D. Lee, H. Nam, M. Won Seo, S. Hoon Lee, D. Tokmurzin, S. Wang, Y.K. Park, Recent progress in the catalytic thermochemical conversion process of biomass for biofuels, Chem. Eng. J. 447 (2022) 137501, https://doi.org/10.1016/j.cej.2022.137501.

[5] S.Y. Foong, R.K. Liew, Y. Yang, Y.W. Cheng, P.N.Y. Yek, W.A. Wan Mahari, X. Y. Lee, C.S. Han, D.V.N. Vo, Q. Van Le, M. Aghbashlo, M. Tabatabaei, C. Sonne, W. Peng, S.S. Lam, Valorization of biomass waste to engineered activated biochar by microwave pyrolysis: Progress, challenges, and future directions, Chem. Eng. J. 389 (2020) 124401, https://doi.org/10.1016/j.cej.2020.124401.

[6] J.J. Chew, V. Doshi, Recent advances in biomass pretreatment - torrefaction fundamentals and technology, Renew. Sustain. Energy Rev. 15 (2011) 4212–4222, https://doi.org/10.1016/j.rser.2011.09.017.

[7] K.A. Abdulyekeen, A.A. Umar, M.F.A. Patah, W.M.A.W. Daud, Torrefaction of biomass: production of enhanced solid biofuel from municipal solid waste and other types of biomass, Renew. Sustain. Energy Rev. 150 (2021) 111436, https://doi.org/10.1016/j.rser.2021.111436.

[8] X. Zhu, Z. Luo, R. Diao, X. Zhu, Combining torrefaction pretreatment and co-pyrolysis to upgrade biochar derived from bio-oil distillation residue and walnut shell, Energy Convers. Manag. 199 (2019) 111970, https://doi.org/10.1016/j.enconman.2019.111970.

[9] M.A. Sukiran, F. Abnisa, W.M.A. Wan Daud, N. Abu Bakar, S.K. Loh, A review of torrefaction of oil palm solid wastes for biofuel production, Energy Convers. Manag. 149 (2017) 101–120, https://doi.org/10.1016/j.enconman.2017.07.011.

[10] A. Leontiev, B. Kichatov, A. Korshunov, A. Kiverin, V. Zaichenko, G. Sytchev, K. Melnikova, Oxidative torrefaction of pine pellets in the quiescent layer of mineral filler, Fuel Process. Technol. 182 (2018) 113–122, https://doi.org/10.1016/j.fuproc.2018.10.021.

[11] A. Sarvaramini, G.P. Assima, F. Larachi, Dry torrefaction of biomass - torrefied products and torrefaction kinetics using the distributed activation energy model, Chem. Eng. J. 229 (2013) 498–507, https://doi.org/10.1016/j.cej.2013.06.056.

[12] Q.V. Bach, W.H. Chen, S.C. Lin, H.K. Sheen, J.S. Chang, Wet torrefaction of microalga Chlorella vulgaris ESP-31 with microwave-assisted heating, Energy Convers. Manag. 141 (2017) 163–170, https://doi.org/10.1016/j.enconman.2016.07.035.

[13] M. Soh, F.J.F. Phang, Y.H. Chai, J.J. Chew, S.K. Loh, S. Yusup, A. Yu, J. Sunarso, Reaction mechanisms of the wet torrefaction of oil palm trunks under the effect of initial pressurisation, Chem. Eng. Res. Des. 193 (2023) 493–506, https://doi.org/10.1016/j.cherd.2023.04.007.

[14] Q.V. Bach, O. Skreiberg, Upgrading biomass fuels via wet torrefaction: a review and comparison with dry torrefaction, Renew. Sustain. Energy Rev. 54 (2016) 665–677, https://doi.org/10.1016/j.rser.2015.10.014.

[15] Y. Wu, C. Dong, H. Wang, J. Peng, Y. Li, C. Samart, M. Ding, One-pot ethanol production from cellulose transformation over multifunctional Pt/WOx and hollow PT@HZSM-5 catalysts, ACS Sustain. Chem. Eng. 10 (2022) 2802–2810, https://doi.org/10.1021/acssuschemeng.1c08204.

[16] X. Zhuang, H. Wang, S. Jiang, X. Hu, T. Su, X. Zhang, L. Ma, A review on the chemo-catalytic conversion of cellulose to bio-ethanol, Green Chem. Eng. (2023), https://doi.org/10.1016/j.gce.2023.08.002.

[17] R. Weingarten, W.C. Conner, G.W. Huber, Production of levulinic acid from cellulose by hydrothermal decomposition combined with aqueous phase dehydration with a solid acid catalyst, Energy Environ. Sci. 5 (2012) 7559, https://doi.org/10.1039/c2ee21593d.

[18] Q. Liu, H. Wang, H. Xin, C. Wang, L. Yan, Y. Wang, Q. Zhang, X. Zhang, Y. Xu, G. W. Huber, L. Ma, Selective cellulose hydrogenolysis to ethanol using NI@C combined with phosphoric acid catalysts, ChemSusChem. 12 (2019) 3977–3987, https://doi.org/10.1002/cssc.201901110.

[19] M. Yang, H. Qi, F. Liu, Y. Ren, X. Pan, L. Zhang, X. Liu, H. Wang, J. Pang, M. Zheng, A. Wang, T. Zhang, One-pot production of cellulosic ethanol via tandem catalysis over a multifunctional Mo/Pt/WOx catalyst, Joule. 3 (2019) 1937–1948, https://doi.org/10.1016/j.joule.2019.05.020.

[20] C. Li, G. Xu, C. Wang, L. Ma, Y. Qiao, Y. Zhang, Y. Fu, One-pot chemocatalytic transformation of cellulose to ethanol over ru-WOx/HZSM-5, Green Chem. 21 (2019) 2234–2239, https://doi.org/10.1039/c9gc00719a.

[21] A. Morone, M. Apte, R.A. Pandey, Levulinic acid production from renewable waste resources: bottlenecks, potential remedies, advancements and applications, Renew. Sustain. Energy Rev. 51 (2015) 548–565, https://doi.org/10.1016/j.rser.2015.06.032.

[22] X. Xu, B. Liang, Y. Zhu, J. Chen, T. Gan, H. Hu, Y. Zhang, Z. Huang, Y. Qin, Direct and efficient conversion of cellulose to levulinic acid catalyzed by carbon foam-supported heteropolyacid with brønsted-Lewis dual-acidic sites, Bioresour. Technol. 387 (2023) 129600, https://doi.org/10.1016/j.biortech.2023.129600.

[23] S.S. Chen, I.K.M. Yu, D.C.W. Tsang, A.C.K. Yip, E. Khan, L. Wang, Y.S. Ok, C. S. Poon, Valorization of cellulosic food waste into levulinic acid catalyzed by heterogeneous br ønsted acids: temperature and solvent effects, Chem. Eng. J. 327 (2017) 328–335, https://doi.org/10.1016/j.cej.2017.06.108.

[24] M. Xiang, J. Liu, W. Fu, T. Tang, D. Wu, Improved activity for cellulose conversion to levulinic acid through hierarchization of ETS-10 zeolite, ACS Sustain. Chem. Eng. 5 (2017) 5800–5809, https://doi.org/10.1021/acssuschemeng.7b00529.

[25] K. Wang, J. Jiang, X. Liang, H. Wu, J. Xu, Direct conversion of cellulose to levulinic acid over multifunctional sulfonated humins in sulfolane-water solution, ACS Sustain. Chem. Eng. 6 (2018) 15092–15099, https://doi.org/10.1021/acssuschemeng.8b03558.

[26] R. García, C. Pizarro, A.G. Lavín, J.L. Bueno, Biomass proximate analysis using thermogravimetry, Bioresour. Technol. 139 (2013) 1–4, https://doi.org/10.1016/j.biortech.2013.03.197.

[27] X. Li, Z. Lu, J. Chen, X. Chen, Y. Jiang, J. Jian, S. Yao, Effect of oxidative torrefaction on high temperature combustion process of wood sphere, Fuel. 286 (2021) 119379, https://doi.org/10.1016/j.fuel.2020.119379.

[28] X. Niu, Y. Xu, L. Shen, Effect of torrefaction on the evolution of carbon and nitrogen during chemical looping gasification of rapeseed cake, Chem. Eng. J. 450 (2022) 138134, https://doi.org/10.1016/j.cej.2022.138134.

[29] D. Chen, A. Gao, K. Cen, J. Zhang, X. Cao, Z. Ma, Investigation of biomass torrefaction based on three major components: hemicellulose, cellulose, and lignin, Energy Convers. Manag. 169 (2018) 228–237, https://doi.org/10.1016/j.enconman.2018.05.063.

[30] C. Zhang, S.H. Ho, W.H. Chen, Y. Xie, Z. Liu, J.S. Chang, Torrefaction performance and energy usage of biomass wastes and their correlations with torrefaction severity index, Appl. Energy. 220 (2018) 598–604, https://doi.org/10.1016/j.apenergy.2018.03.129.

[31] L. Segal, J.J. Creely, A.E. Martin, C.M. Conrad, An empirical method for estimating the degree of crystallinity of native cellulose using the X-ray diffractometer, Text. Res. J. 29 (1959) 786–794, https://doi.org/10.1177/004051755902901003.

[32] A. Thygesen, J. Oddershede, H. Lilholt, A.B. Thomsen, K. Ståhl, On the determination of crystallinity and cellulose content in plant fibres, Cellulose. 12 (2005) 563–576, https://doi.org/10.1007/s10570-005-9001-8.

[33] N. Johar, I. Ahmad, A. Dufresne, Extraction, preparation and characterization of cellulose fibres and nanocrystals from rice husk, Ind. Crops Prod. 37 (2012) 93–99, https://doi.org/10.1016/j.indcrop.2011.12.016.

[34] G. SriBala, R. Chennuru, S. Mahapatra, R. Vinu, Effect of alkaline ultrasonic pretreatment on crystalline morphology and enzymatic hydrolysis of cellulose, Cellulose. 23 (2016) 1725–1740, https://doi.org/10.1007/s10570-016-0893-2.

[35] A. Zheng, Z. Zhao, S. Chang, Z. Huang, K. Zhao, G. Wei, F. He, H. Li, Comparison of the effect of wet and dry torrefaction on chemical structure and pyrolysis behavior of corncobs, Bioresour. Technol. 176 (2015) 15–22, https://doi.org/10.1016/j.biortech.2014.10.157.

[36] A. Kostyniuk, D. Bajec, B. Likozar, Catalytic hydrogenation, hydrocracking and isomerization reactions of biomass tar model compound mixture over ni-modified zeolite catalysts in packed bed reactor, Renew. Energy. 167 (2021) 409–424, https://doi.org/10.1016/j.renene.2020.11.098.

[37] L. Zhu, Z. Hu, M. Huang, H. Peng, W. Zhang, D. Chen, Z. Ma, Valorisation of cotton stalk toward bio-aromatics: effect of wet torrefaction deoxygenation and deminerization pretreatment on catalytic fast pyrolysis using ga modified hierarchical zeolite, Fuel. 330 (2022) 125571, https://doi.org/10.1016/j.fuel.2022.125571.

[38] M.F. Li, Y. Shen, J.K. Sun, J. Bian, C.Z. Chen, R.C. Sun, Wet torrefaction of bamboo in hydrochloric acid solution by microwave heating, ACS Sustain. Chem. Eng. 3 (2015) 2022–2029, https://doi.org/10.1021/acssuschemeng.5b00296.

[39] D. Lašič Jurković, A. Kostyniuk, B. Likozar, Mechanisms, reaction micro-kinetics and modelling of hydrocracking of aromatic biomass tar model compounds into benzene, toluene and xylenes (BTX) over H-ZSM-5 catalyst, Chem. Eng. J. 445 (2022), https://doi.org/10.1016/j.cej.2022.136898.

[40] C. He, C. Tang, C. Li, J. Yuan, K.Q. Tran, Q.V. Bach, R. Qiu, Y. Yang, Wet torrefaction of biomass for high quality solid fuel production: a review, Renew. Sustain. Energy Rev. 91 (2018) 259–271, https://doi.org/10.1016/j.rser.2018.03.097.

[41] D. Chen, K. Cen, F. Chen, Y. Zhang, Solar pyrolysis of cotton stalks: combined effects of torrefaction pretreatment and HZSM-5 zeolite on the bio-fuels upgradation, Energy Convers. Manag. 261 (2022) 115640, https://doi.org/10.1016/j.enconman.2022.115640.

[42] L. Dai, C. He, Y. Wang, Y. Liu, Z. Yu, Y. Zhou, L. Fan, D. Duan, R. Ruan, Comparative study on microwave and conventional hydrothermal pretreatment of bamboo sawdust: hydrochar properties and its pyrolysis behaviors, Energy Convers. Manag. 146 (2017) 1–7, https://doi.org/10.1016/j.enconman.2017.05.007.

[43] Y. Wang, Q. Wu, L. Dai, Z. Zeng, Y. Liu, R. Ruan, G. Fu, Z. Yu, L. Jiang, Co-pyrolysis of wet torrefied bamboo sawdust and soapstock, J. Anal. Appl. Pyrolysis. 132 (2018) 211–216, https://doi.org/10.1016/j.jaap.2018.02.012.

[44] S. Zhang, T. Chen, Y. Xiong, Q. Dong, Effects of wet torrefaction on the physicochemical properties and pyrolysis product properties of rice husk, Energy Convers. Manag. 141 (2017) 403–409, https://doi.org/10.1016/j.enconman.2016.10.002.

[45] X. Wang, J. Wu, Y. Chen, A. Pattiya, H. Yang, H. Chen, Comparative study of wet and dry torrefaction of corn stalk and the effect on biomass pyrolysis polygeneration, Bioresour. Technol. 258 (2018) 88–97, https://doi.org/10.1016/j.biortech.2018.02.114.

[46] J. Jian, Z. Lu, S. Yao, X. Li, W. Song, Comparative study on pyrolysis of wet and dry torrefied beech wood and wheat straw, Energy and Fuels. 33 (2019) 3267–3274, https://doi.org/10.1021/acs.energyfuels.8b04501.

[47] Q. Ma, L. Han, G. Huang, Effect of water-washing of wheat straw and hydrothermal temperature on its hydrochar evolution and combustion properties, Bioresour. Technol. 269 (2018) 96–103, https://doi.org/10.1016/j.biortech.2018.08.082.

[48] Q.V. Bach, K.Q. Tran, Ø. Skreiberg, T.T. Trinh, Effects of wet torrefaction on pyrolysis of woody biomass fuels, Energy. 88 (2015) 443–456, https://doi.org/10.1016/j.energy.2015.05.062.

[49] M. Volpe, L. Fiori, From olive waste to solid biofuel through hydrothermal carbonisation: the role of temperature and solid load on secondary char formation and hydrochar energy properties, J. Anal. Appl. Pyrolysis. 124 (2017) 63–72, https://doi.org/10.1016/j.jaap.2017.02.022.

[50] P. Gao, Y. Zhou, F. Meng, Y. Zhang, Z. Liu, W. Zhang, G. Xue, Preparation and characterization of hydrochar from waste eucalyptus bark by hydrothermal carbonization, Energy. 97 (2016) 238–245, https://doi.org/10.1016/j.energy.2015.12.123.

[51] G.K. Parshetti, S. Kent Hoekman, R. Balasubramanian, Chemical, structural and combustion characteristics of carbonaceous products obtained by hydrothermal carbonization of palm empty fruit bunches, Bioresour. Technol. 135 (2013) 683–689, https://doi.org/10.1016/j.biortech.2012.09.042.

[52] M. Pala, I.C. Kantarli, H.B. Buyukisik, J. Yanik, Hydrothermal carbonization and torrefaction of grape pomace: a comparative evaluation, Bioresour. Technol. 161 (2014) 255–262, https://doi.org/10.1016/j.biortech.2014.03.052.

[53] A. Missaoui, S. Bostyn, V. Belandria, B. Cagnon, B. Sarh, I. Gökalp, Hydrothermal carbonization of dried olive pomace: energy potential and process performances, J. Anal. Appl. Pyrolysis. 128 (2017) 281–290, https://doi.org/10.1016/j.jaap.2017.09.022.

[54] D. Chu, Y. Xin, C. Zhao, Production of bio-ethanol by consecutive hydrogenolysis of corn-stalk cellulose, chinese, J. Catal. 42 (2021) 844–854, https://doi.org/10.1016/S1872-2067(20)63709-3.

[55] H. Song, P. Wang, S. Li, W. Deng, Y. Li, Q. Zhang, Y. Wang, Direct conversion of cellulose into ethanol catalysed by a combination of tungstic acid and zirconia-supported pt nanoparticles, Chem. Commun. 55 (2019) 4303–4306, https://doi.org/10.1039/c9cc00619b.

[56] Z. Su, J. Zhang, S. Lu, F.S. Xiao, Pt nanoparticles supported on nb-modified TiO2 as an efficient heterogeneous catalyst for the conversion of cellulose to light bioalcohols, Chem. Commun. 58 (2022) 12349–12352, https://doi.org/10.1039/d2cc03845e.

[57] N. Karanwal, R.G. Kurniawan, J. Park, D. Verma, S. Oh, S.M. Kim, S.K. Kwak, J. Kim, One-pot, cascade conversion of cellulose to γ-valerolactone over a multifunctional Ru–Cu/zeolite-Y catalyst in supercritical methanol, Appl. Catal. B Environ. 314 (2022) 121466, https://doi.org/10.1016/j.apcatb.2022.121466.

[58] C. Ma, B. Cai, L. Zhang, J. Feng, H. Pan, Acid-catalyzed conversion of cellulose into levulinic acid with biphasic solvent system, Front. Plant Sci. 12 (2021), https://doi.org/10.3389/fpls.2021.630807.

[59] X. Li, R. Xu, J. Yang, S. Nie, D. Liu, Y. Liu, C. Si, Production of 5-hydroxymethyl-furfural and levulinic acid from lignocellulosic biomass and catalytic upgradation, Ind. Crops Prod. 130 (2019) 184–197, https://doi.org/10.1016/j.indcrop.2018.12.082.

[60] G. Yang, E.A. Pidko, E.J.M. Hensen, Mechanism of bronsted acid-catalyzed conversion of carbohydrates, J. Catal. 295 (2012) 122–132, https://doi.org/10.1016/j.jcat.2012.08.002.

[61] Z. Sun, L. Xue, S. Wang, X. Wang, J. Shi, Single step conversion of cellulose to levulinic acid using temperature-responsive dodeca-aluminotungstic acid catalysts, Green Chem. 18 (2016) 742–752, https://doi.org/10.1039/c5gc01730k.

[62] N.A.S. Ramli, N.A.S. Amin, Optimization of renewable levulinic acid production from glucose conversion catalyzed by FE/HY zeolite catalyst in aqueous medium, Energy Convers. Manag. 95 (2015) 10–19, https://doi.org/10.1016/j.enconman.2015.02.013.

[63] M. Mikola, J. Ahola, J. Tanskanen, Production of levulinic acid from glucose in sulfolane/water mixtures, Chem. Eng. Res. Des. 148 (2019) 291–297, https://doi.org/10.1016/j.cherd.2019.06.022.